

Automated neuroradiological support systems for multiple cerebrovascular disease markers - A systematic review and meta-analysis

Jesse Phitidis^{a,b,*}, Alison Q O'Neil^{b,c}, William N Whiteley^a, Beatrice Alex^{d,e}, Joanna M. Wardlaw^{a,f}, Miguel O. Bernabeu^g, Maria Valdés Hernández^{a,f}

^a*Centre for Clinical Brain Sciences, University of Edinburgh, 49 Little France Crescent, Edinburgh, EH164SB, United Kingdom*

^b*Canon Medical Research Europe, Bonnington Bond, 2 Anderson Place, Edinburgh, EH65NP, United Kingdom*

^c*School of Engineering, University of Edinburgh, Sanderson Building, Edinburgh, EH93FB, United Kingdom*

^d*School of Literature, Languages and Culture, University of Edinburgh, 50 George Square, Edinburgh, EH89JY, United Kingdom*

^e*Edinburgh Futures Institute, University of Edinburgh, 1 Lauriston Place, Edinburgh, EH39EF, United Kingdom*

^f*UK Dementia Research Institute, Centre at The University of Edinburgh, 49 Little France Crescent, Edinburgh, EH164SB, United Kingdom*

^g*Usher Institute, University of Edinburgh, NINE, 9 Little France Road, Edinburgh, EH164UX, United Kingdom*

Abstract

Cerebrovascular diseases (CVD) can lead to stroke and dementia. Stroke is the second leading cause of death world wide and dementia incidence is increasing by the year. There are several markers of CVD that are visible on brain imaging, including: white matter hyperintensities (WMH), acute and chronic ischaemic stroke lesions (ISL), lacunes, enlarged perivascular spaces (PVS), acute and chronic haemorrhagic lesions, and cerebral microbleeds (CMB). Brain atrophy also occurs in CVD. These markers are important for patient management and intervention, since they indicate elevated risk of future stroke and dementia. We systematically reviewed automated systems de-

*Corresponding author

Email address: j.phitidis@ed.ac.uk (Jesse Phitidis)

signed to support radiologists reporting on these CVD imaging findings. We considered commercially available software and research publications which identify *at least two* CVD markers. In total, we included 29 commercial products and 13 research publications. Two distinct types of commercial support system were available: those which identify acute stroke lesions (haemorrhagic and ischaemic) from computed tomography (CT) scans, mainly for the purpose of patient triage; and those which measure WMH and atrophy regionally and longitudinally. In research, WMH and ISL were the markers most frequently analysed together, from magnetic resonance imaging (MRI) scans; lacunes and PVS were each targeted only twice and CMB only once. For stroke, commercially available systems largely support the emergency setting, whilst research systems consider also follow-up and routine scans. The systems to quantify WMH and atrophy are focused on neurodegenerative disease support, where these CVD markers are also of significance. There are currently no openly validated systems, commercially, or in research, performing a comprehensive joint analysis of all CVD markers (WMH, ISL, lacunes, PVS, haemorrhagic lesions, CMB, and atrophy).

Keywords: Cerebrovascular disease, neuroradiology, machine learning

1. Introduction

Stroke is the second leading cause of death globally (Feigin et al., 2021), with 6.5 million deaths resulting from 12.2 million annual reported occurrences (Feigin et al., 2022). Given the high morbidity of stroke, with almost 50% of sufferers being left disabled, prevention is of paramount importance. Epidemiological studies have identified several risk factors for stroke, most of which are modifiable. Amongst them are hypertension, diabetes mellitus, hypercholesterolaemia, cardiovascular diseases, and smoking (Donkor et al., 2018), all which have been associated with cerebrovascular disease (CVD) markers identifiable through different medical imaging modalities. CVD markers include ischaemic stroke lesions (ISL), haemorrhagic stroke lesions, white matter hyperintensities (WMH), cerebral microbleeds (CMB), lacunes, enlarged perivascular spaces (PVS), brain aneurysms (BA), and brain atrophy. In turn, previous stroke or the presence of CVD markers have been linked with increased risk of future stroke (Arboix, 2015; Debette and Markus, 2010), while CVD markers have also been associated with dementia (Tanabe, 2011). CVD is thought to be a “whole-brain disease” (Shi

and Wardlaw, 2016; Duering et al., 2023), therefore, the simultaneous identification of all possible CVD markers can play a valuable role in enabling appropriate preventative measures and lifestyle modifications.

There is a worldwide shortage of radiologists (Henderson, 2022), and software systems to support image interpretation are a potential solution. Not only this, but automation has the means to reduce the variability of interpretations seen amongst radiologists. CVD marker assessment differs by imaging modality, since different CVD marker subsets are visible in different imaging modalities. For instance, computed tomography (CT) scans may be used to assess lacunes and WMH, whilst magnetic resonance imaging (MRI) scans show more soft tissue detail and may be used to assess lacunes, WMH, PVS, CMB, and ISL. Any neuroradiological support system for CVD should provide information on all visible markers of CVD in the target image modality. In this systematic review, we define a *complete CVD support system* as one which is able to identify and assess lacunes, WMH, PVS, CMB, and ISL from one or more medical imaging scans.

Previous reviews have examined computational neuroradiology support systems (Olthof et al., 2020; Yearley et al., 2023; Yao et al., 2020), stroke support systems (Wardlaw et al., 2022; Soun et al., 2021; Bivard et al., 2020; Yeo et al., 2021; Mikhail et al., 2020; Murray et al., 2020; Abbasi et al., 2023), WMH detection systems (Balakrishnan et al., 2021), CMB detection systems (Ferlin et al., 2023), and PVS detection systems (Barisano et al., 2022; Pham et al., 2022; Waymont et al., 2024). Jiang et al. (2022) performed a systematic review on computational extraction of three cerebral small vessel disease (cSVD) markers visible on MRI: PVS, CMB and lacunes. They found that good performance was achieved in small private datasets, but no pipeline has been validated in larger more heterogeneous datasets.

Importantly, images from cSVD patients are likely to have multiple markers which confound each other due to similar appearance (e.g. PVS and lacunes or ISL and WMH), presenting a real challenge to automated detection. In this systematic review, we identify both commercially available systems and research publications on fully automatic methods, software products or platforms, which assess *multiple* CVD markers, and meta-analyse their scope and characteristics.

2. Methods

We jointly perform a systematic review of commercial systems and research publications. In this section we describe our selection, search, and analysis methods.

2.1. Selection strategy

We selected relevant works according to the criteria below.

Inclusion criteria. The primary inclusion criterion was that the commercial system or primary publication must present a method, software or platform that *fully automatically* assesses *multiple* CVD markers from radiological brain images. Methods that only aimed at segmenting, quantifying or scoring 1 CVD feature, but in the process also identified other confounding CVD features for exclusion, were considered to qualify as identifying multiple CVD markers. This restriction on the number of CVD markers served to reduce the results to a manageable volume whilst focusing in on the most relevant systems for assessing such a complex, multifaceted disease. Research publications included only peer-reviewed full papers.

Exclusion criteria. The following were excluded:

- Semi-automated methods
- Abstracts, where an associated full paper was not available (research systems)
- Non-peer-reviewed publications (research systems)
- Publications with no evaluation against ground truth (research systems)
- Non-English language publications (research systems)
- Products from companies with non-English language websites/materials without a translation available (commercial systems)
- Animal studies

2.2. Search strategy

We followed different strategies for identifying commercial systems and research publications, as detailed below.

2.2.1. Searching for commercial systems

We used multiple sources to review companies who were active in the period October 2022 to October 2024, which might develop products fitting the inclusion criteria. We reviewed companies:

- mentioned in [Wardlaw et al. \(2022\)](#)'s evaluation of the accuracy of automated stroke diagnosis systems
- mentioned in [Olthof et al. \(2020\)](#)'s review of AI in neuroradiology
- listed on the website <https://grand-challenge.org/aiforradiology/> (describing products related to AI in radiology) which were categorised as "neuro"
- who had exhibited at the Radiological Society of North America (RSNA) (<https://www.rsna.org/>) in 2021, 2022 or 2023 (other conferences were also considered but rejected due to significant overlap)

To decide whether any product from a company met the inclusion criteria, we carefully checked the websites and online materials related to the relevant product, as well as checking the US Food and Drug Administration (FDA) 510(k) pre-market notification documents where possible, since this often contains details not found elsewhere.

2.2.2. Searching for research publications

The literature search was carried out on Web of Science (<https://www.webofscience.com/wos/woscc/>). The search (conducted on 18/09/2024) included papers published between 2008 and September 2024, which mention at least 2 CVD features as well as referencing automation or machine learning. The start date was chosen because we are interested in systems with reasonable performance by today's standards, and 16 years of advancement in computer vision and the advent of deep learning likely render prior works - although potentially methodologically interesting - less relevant in the absence of a more recent update or enhancement.

The combination of search terms used in the advanced search was:

((white matter hyper AND lacune*) OR (white matter hyper* AND (infarct OR stroke)) OR (white matter hyper* AND (perivascular spaces OR Virchow-Robin)) OR (white matter hyper* AND microbleed) OR (lacune**

AND (infarct OR stroke)) OR (lacune AND (perivascular spaces OR Virchow-Robin)) OR (lacune* AND microbleed) OR ((infarct OR stroke) AND (perivascular spaces OR Virchow-Robin)) OR ((infarct OR stroke) AND microbleed) OR ((perivascular spaces OR Virchow-Robin) AND microbleed)) AND (segment* OR classifier OR machine learning OR deep learning OR ai OR auto* quantif*)*

Abstracts were screened to identify articles likely to meet the inclusion criteria. The full text of these articles was then inspected to produce the final list of included research publications. Articles from authors' personal libraries known to meet the inclusion criteria and not identified in the literature search were also added to the final list.

2.3. Data extraction

For each neuroradiology support system, we extracted information regarding: the modalities/sequences used; the pathologies targeted; the specific features of the system (e.g. segmentation); development and validation data characteristics and reference standard; the method/training details; the validation details; and obtained regulatory approvals (for commercial systems only).

For the commercial systems, the information comes from the company website, white papers, explicitly cited publications, and FDA pre-market notifications. Where information was lacking about methods and training data, a further search was performed including review of linked publications. Where a company offered sub-products making up a more comprehensive product, the complete product was considered, and the features were considered to be the combination of the features of the sub-products. However, where sensible, information was reported for each sub-product.

2.4. Analysis of bias risks and applicability

We used a version of the QUADAS 2 tool which is used to assess risk of bias and applicability in systematic reviews.¹ This table is commonly presented with the entries “low”, “unclear”, and “high”. However, since a high risk of bias is bad, but a high applicability is good, we chose to use “good”, “medium”, and “bad” as categories. An example of an entry where

¹<https://www.bristol.ac.uk/media-library/sites/quadas/migrated/documents/quadas2.pdf>

“bad” would be given is in the question “Is the ref std. likely to be correct?” if the ground truth was automatically generated.

3. Results

3.1. Search results

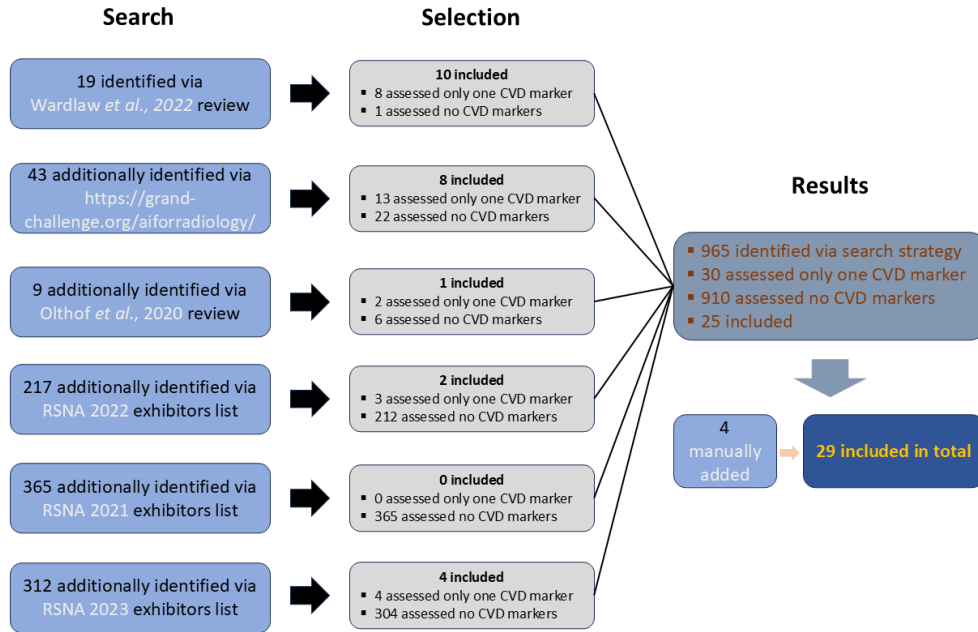
Fig 1 shows the results of the data collection process. In total, 965 commercial systems were identified as candidates, but after applying the inclusion criteria, only 25 remained. 30 of the 965 systems were rejected because they evaluated only 1 CVD marker and the remainder were rejected because they did not evaluate any of the CVD markers. In total 29 systems were considered after manually including 4 systems known to the authors, which were not identified as part of the search strategy. After screening the abstracts of 745 research publications, 16 were selected for full text screening and 9 passed the inclusion criteria. Additionally, 4 papers from authors’ personal libraries were included.

3.2. Commercial systems

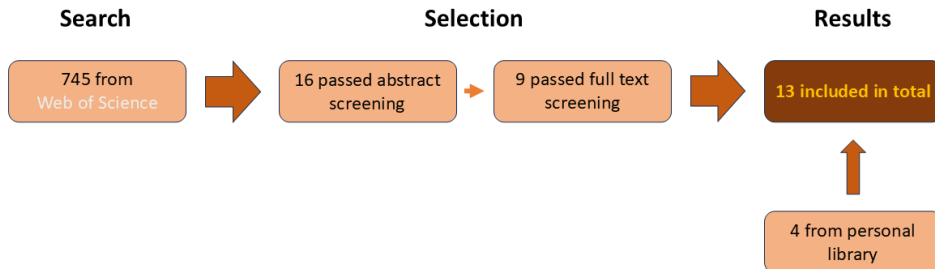
The results of reviewing the 29 identified products can be seen in **Table 1**. Products broadly fall into 2 categories: stroke detection systems and general neuroradiology support systems with emphasis on neurodegenerative diseases. Below we summarise the types of CVD markers and imaging modalities that these products support, characteristics of the data used in development/testing, deep learning methods applied, regulatory approval, and the availability of validation information. More detail, including information about the reference standard and product impact, is provided in the supplementary material.

3.2.1. CVD markers and imaging modalities

Stroke systems. The 19 stroke detection systems (Always-on AI, Enterprise CTB, Cina, e-Stroke, BrainScan CT, Cercare Stroke, APOLLO BRAIN, DeepCT, icobrain, NeuroShield CT-TBI, MEDIHUB STROKE, Stroke Suite, Stroke-Viewer, qER, Rapid Stroke, Digital Brain, Viz Radiology Suite, Stro-Care Suite, uAI Discover IschaemicStroke/ICH) place emphasis on rapid identification and triage of acute stroke, i.e. identifying ischaemic stroke lesions (ISL) and intracranial haemorrhages (ICH). This can be seen in the co-occurrence matrix in **Fig 2b** displaying the number of paired CVD markers, which shows that 12 systems assess both haemorrhagic strokes and ischaemic



(a) Data collection process and results for commercially available CVD support systems with selection based on the inclusion/exclusion criteria



(b) Data collection process and results for research publications on CVD support systems with selection based on the inclusion/exclusion criteria

Figure 1

stroke lesions (i.e. ICH and ISL), and 10 assess both haemorrhagic strokes and occlusion in large vessels (i.e. ICH and LVO). Both ISL and large vessel occlusion (LVO) are indicators of ischaemic stroke; LVO detection identifies the location of the blocked vessel and specifically the blockage (usually from CT angiogram (CTA) which uses contrast injection to show the vessels), whilst ISL detection systems show areas of ischaemic tissue (which may not

necessarily be limited to the site of the occlusion).

Consistent with the interest in diagnosing the cause of acute stroke, 17/19 systems target non-contrast CT (NCCT), which is a widely used imaging modality for acute stroke world wide. Of these, 8/17 systems assess the Alberta stroke program early CT score (ASPECTS) (Barber et al., 2000) and outline the area of hypoattenuation (which corresponds to the ISL marker). Then, 8/17 systems target CT perfusion (CTP) to segment the ISL core. Finally, 10 systems target CT angiograms (CTA) for detecting or localising occlusion in large vessels (LVO), and 4 systems detect aneurysms from CTA.

Overall, Enterprise CTB from annalise.ai appears to be the most comprehensive system, detecting 6 CVD markers amongst the 130 it assesses in NCCT scans. However, this includes PVS which is typically best identified on MRI (not NCCT), and there is no available validation data on PVS and some of the other markers. uAI Discover from United Imaging Intelligence also claims to assess 6 CVD markers, although no further information regarding the product’s application or validation was found.

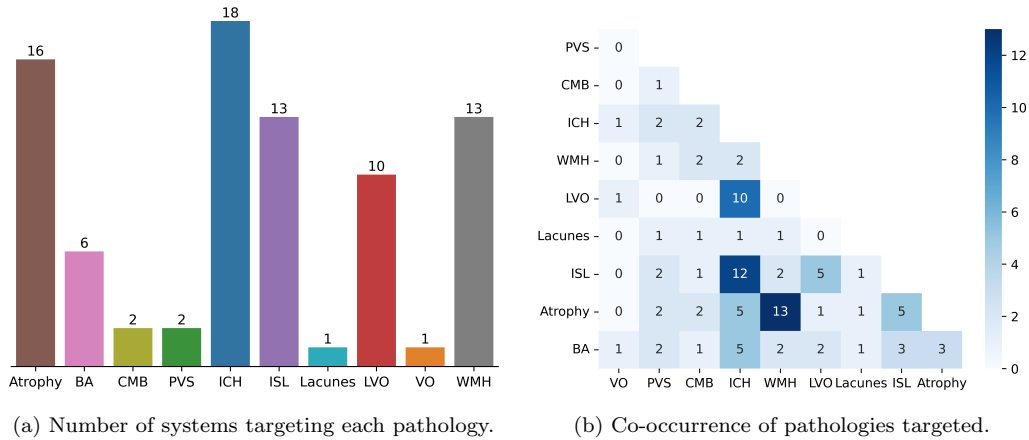


Figure 2: Distribution of pathologies targeted by the identified commercial systems.

General neuroradiology systems. There were 16 systems that quantify brain atrophy and/or WMH (Enterprise CTB, BrainScan CT, cMRI, NeuroQuant, icobrain, NeuroShield MR, mdbrain, AQUA, Pixyl.Neuro, Quantib ND, NEUROCLOUD VOL, DeepBrain, AgingCare Suite, QP-Brain, QyScore, UAI Discover CSVD). Although these systems are mostly intended to support diagnosis of diseases such as dementia, they have been included in our review

since brain atrophy and WMH are also markers of CVD. All these systems except for Enterprise CTB and BrainScan CT use MRI (T1 and/or FLAIR explicitly mentioned for all products with the exception of NeuroShield, QUANTIB ND and UAI Discover CSVD). 12/16 systems provide atrophy quantification by region (9 perform longitudinal analysis) and the same number provide WMH segmentation and volumes. 5 systems provide regional FLAIR-hyperintense volumes in periventricular, juxtacortical/cortical, infratentorial, and the spinal cord (if any).

3.2.2. Sample characteristics

Development. Information on training/development data was found for at least 1 sub-product in 15/29 systems. The median dataset size was 2869 subjects and the maximum was 12.5 million (BrainScan CT). In 9/15 systems, the use of data from multiple scanners or sites was stated for at least 1 sub-product, while at least 1 sub-product in 2/15 and 3/15 described the age and sex characteristics respectively.

Validation. Information on validation data was found for at least 1 sub-product in 19/29 systems. The median dataset size was 270 subjects and the maximum was 3363 (Enterprise CTB). The use of multiple scanners or sites was mentioned by at least 1 sub-product in 12/19 systems and the sex and age characteristics were detailed for at least 1 sub-product by 7/19.

3.2.3. Deep learning methods

18/29 systems utilise deep learning (DL) methods in at least 1 of their sub-products. Of these, all deploy convolutional neural networks (CNNs) (LeCun et al., 1989), with 1 product (Enterprise CTB) also making use of the vision transformer architecture (ViT) (Dosovitskiy et al., 2020). Of the 27 sub-products using CNNs, 9 state the use of a U-Net based model (Ronneberger et al., 2015) and 9 state that a 3D architecture is used. 9 sub-products utilised multiple models with at least 1 being a DL model, in multi-stage pipelines or ensembles. Of these, 7 described the purpose of each model. Details regarding at least 1 aspect of the training process (e.g. data augmentation, loss function, optimiser, data sampling, etc) were found for 5 sub-products. Of the 19 systems assessing stroke, 15 utilise DL in at least 1 sub-product while 5/16 of the systems offering WMH or atrophy segmentation/quantification use DL.

3.2.4. Validation and regulatory approval

A full analysis of all internal or external validation studies for each product was outside the scope of this review, but we refer the interested reader to [Yearley et al. \(2023\)](#).

Of the 50 sub-products for which validation metrics were found, 28 provided sensitivity and specificity (13 with confidence intervals), 9 reported area under the receiver operating characteristic curve (AUC), and 17 reported Dice similarity coefficient (DSC). The most frequently claimed clinical impact was a reduction in time required for the patient workflow, which was stated by 12 subsystems.

Of the 29 systems identified, 19 have at least 1 sub-product which is FDA approved and 26 have at least 1 sub-product with CE marking.

Table 1: Commercial systems - overview. Some products include additional non-CVD related features not mentioned here (e.g. assessment of cranial fracture or glioma).

Pathologies and anatomy:

ICH: intracerebral haemorrhage, (L)VO: (large) vessel occlusion, BA: brain aneurysm, ISL: ischaemic stroke lesion, PVS: enlarged perivascular spaces, SVD: small vessel disease, WMH: white matter hyperintensities, EDH: epidural hematoma, SDH: subdural haemorrhage, SAH: subarachnoid haemorrhage, IVH: intraventricular haemorrhage, IPH: intraparenchymal haemorrhage, ICA: internal carotid artery, MCA: middle cerebral artery.

Modalities:

NCCT: non-contrast computed tomography, CTA: computed tomography angiography, CTP: computed tomography perfusion, MRI: magnetic resonance imaging, T1: T1-weighted MRI, T2: T2-weighted MRI, T2*: T2*-weighted MRI, FLAIR: fluid-attenuated inversion recovery MRI, SWI: susceptibility-weighted imaging MRI, DWI: diffusion-weighted imaging MRI, GRE: gradient echo MRI, TOF: time-of-flight MRI angiography.

Other abbreviations:

AI: artificial intelligence, DL: deep learning, ML: machine learning, RB: rule-based.

(AI is stated as the method class when the company states the product as being AI and further investigation does not clarify the method).

Company	Product	Pathology	Modality	Features	Method class	Approval (sub-product)
aidoc, icometrix	Always-on AI	ICH, VO, M1 LVO, BA	NCCT, CTA, CTP	Identification of suspected findings per pathology. Core segmentation and volume for (M1 L)VO from CTP.	DL	FDA (II), CE (I) (BriefCase ICI triage) (BriefCase LVO triage) (Briefcase BA triage) (icobrain-cva)
annalise.ai	Enterprise CTB	ICH, ISL, BA, atrophy, PVS, SVD, ... (130 total)	NCCT	Detection or segmentation of 130 radiological findings including ICH subtypes, infarcts, PVS, and SVD.	DL	FDA (II), CE (IIb)
Avicenna.AI	Cina	ICH, LVO, ISL	NCCT, CTA	Identification of suspected ICH or LVO. ASPECTS with infarct outline and probability map of hypoattenuation and sulcal effacement.	DL	FDA (II), CE (I) (CINA-ICH) (CINA-LVO) CE (I) (CINA-ASPECTS)

Table 1 continued from previous page

BRAINOMIX	e-Stroke	ICH, LVO, ISL	NCCT, CTA, CTP	ASPECTS with infarct volume and hypoattenuation heat map (hyperattenuation also detected indicating bleeding). Bounding box on CTA for vessel occlusion. Core and penumbra segmentation and volume and mismatch ratio from CTP.	ML, RB, DL	FDA (II), CE (IIa) (e-CTA) CE (IIa) (e-CTP) (e-ASPECTS)
BRAINSCAN.AI	BrainScan CT	ICH, ISL, atrophy	NCCT	Segmentation and probability map of ICH subtypes and acute and chronic ISL as well as areas of atrophy.	AI	CE (IIa)
Cercare Medical	Cercare Stroke	ICH, LVO	NCCT, CTA, MRI	Detects ICH. Identifies and provides volume of infarcted lesions. Identifies exact location of LVO. Perfusion maps from CT or MRI perfusion imaging and additional biomarkers of oxygenation.	DL	CE (IIa)
CEREBRIU	APOLLO BRAIN	ICH, ISL	FLAIR, T2*, SWI, DWI	Detects ICH and ISL.	AI	CE (I)
Combinostics	cMRI	WMH, Atrophy	T1, FLAIR	Segmentation of brain and atrophy per region and WMH per region; longitudinal analysis available. Outputs structured report.	RB	FDA (II), CE (IIa)
cortechs.ai	Neuro-Quant	WMH, atrophy	T1, FLAIR	Brain atrophy per region from T1. Segmentation and volume of WMH and longitudinal analysis from FLAIR.	ML, RB, AI	FDA (II), CE (IIa)
DEEP01	DeepCT	ICH, LVO	NCCT, CTA	Detection of ICH (region, subtype, volume, modified Fisher scale, Marshall score, IMPACT score, midline shift, and Evans index). Detection and localisation of LVO.	DL	FDA (II), CE (I)

Table 1 continued from previous page

icometrix	icobrain	ISL, WMH, atrophy	CTP, T1, FLAIR	Segmentation of ischaemic core and penumbra from CTP. Segmentation and volume and longitudinal analysis of FLAIR hyperintensities and T1 hypointensities. Brain volume change metrics by region from T1.	AI	FDA (II), CE (I)
INMED AI	NeuroShield	ICH, WMH, CMB, atrophy	NCCT, MRI	Brain atrophy by region, WMH and CMBs (no info), detection and segmentation of ICH and triage.	DL	FDA (II) (NeuroShieldMR)
JLK	MEDIHUB STROKE	ICH, ISL	NCCT, CTP, T1, T2, FLAIR, GRE, PWI, DWI	ICH localisation and subtype (EDH, SDH, SAH, IVH, intracerebral) from NCCT. Ischaemic stroke subtype probability from DWI and optional FLAIR, T1, T2. Severity probability according to the NIH stroke scale from DWI. Volume mismatch from DWI/PWI. On-set time prediction and ischaemic core segmentation from DWI/FLAIR. Collateral map analysis, ischaemic core and penumbra volume and mismatch from CTP. Infarct segmentation and prognosis from DWI and early detection from NCCT.	DL, AI	CE (I) (JBS-01K) (JBS-04K)
mediaire	mdbrain	WMH, atrophy, BA	T1, FLAIR, TOF	Brain volume by region and longitudinal changes from T1. Segmentation of WMH and regional assessment and longitudinal changes from T1 /FLAIR. Segmentation of BA from TOF.	DL	CE (I)
Methinks	Stroke Suite	ICH, LVO	NCCT, CTA	Notification of ICH and LVO for patient triage.	DL	CE (I)
neurophet	AQUA	WMH, atrophy	T1, FLAIR	Brain atrophy by region and longitudinal analysis from T1. WMH burden score from FLAIR.	DL	CE (IIa)

Table 1 continued from previous page

NICOLAB	Stroke-Viewer	ICH, LVO, ISL	NCCT, CTA, CTP	Segmentation and volume of ICH and SAH from NCCT. ASPECTS scoring. Identification and bounding box of LVO and collateral score from CTA. Core and mismatch volumes from CTP.	DL, AI	FDA (II), CE (I)
PIXYL	Pixyl.Neuro	WMH, atrophy	T1, FLAIR	Segmentation and volume of WMH by region and longitudinally and brain atrophy by region and longitudinally.	AI	FDA (II), CE (IIa)
Quantib	Quantib ND	WMH, atrophy	MRI	Brain atrophy by region and longitudinal changes. Segmentation of WMH and longitudinal changes.	ML	FDA (II), CE (IIa)
QUBIOtech	NEURO-CLOUD VOL	WMH, atrophy	T1, FLAIR	Brain atrophy quantification by region and longitudinal changes from T1. Segmentation of WMH by region and longitudinal changes from FLAIR.	ML, RB	CE (I)
qure.ai	qER	ICH, ISL	NCCT	Bounding box and volume for ICH subtypes (IPH, IVH, SDH, SAH, EDH). Detects and quantifies midline shift. ASPECTS score and outlines hypoattenuated area. Bounding box for acute and chronic infarcts (including lacunar).	DL	FDA (II), CE (IIa)
RapidAI	Rapid Stroke	ICH, LVO, ISL	NCCT, CTA, CTP	Identification of ICH and segmentation and volume of hyperattenuated region from NCCT. ASPECTS score. Colour coded overlay of regions of blood vessel density asymmetry from CTA. Identification of LVO in the ICA or MCA. Hypoattenuation and mismatch volume from CTP.	ML, DL, AI	FDA (II), CE (I)
SHUKUN	Digital Brain	ICH, BA, ISL	NCCT, CTA	Segments ICH and ischaemia from NCCT. Provides diameter measurements and ASPECTS. Measures dimensions of BA from CTA.	AI	CE (I)

Table 1 continued from previous page

Viz.ai	Viz Radiology Suite	ICH, LVO, BA	NCCT, CTA	Detection of LVO and BA from CTA. Detection of ICH and SDH from NCCT.	DL	FDA (II), CE (I) (Viz LVO) (Viz ICH) FDA (II) (Viz ANEURYSM)
VUNO	DeepBrain	WMH, Atrophy	T1, FLAIR	Brain atrophy per region, WMH, and cortical thickness. Brain structures segmented include 2 vessels.	DL	FDA (II), CE (IIa)
Heuron	StroCare Suite, AgingCare Suite	ICH, LVO, ISL, Atrophy	NCCT, CTA, CTP, T1	ICH detection and triage from NCCT. LVO detection and hemisphere from NCCT. ASPECTS and regional analysis from NCCT. LVO detection and hemisphere from CTA. Volume mismatch from CTP. Atrophy per region from T1.	AI	FDA (II) (StroCare Suite ICH)
Quibim	QP-Brain	WMH, Atrophy	T1, FLAIR	Brain atrophy per region from T1. Segmentation and volume of WMH and longitudinal analysis from FLAIR.	AI, DL	FDA (II), CE (IIb)
QYNAPSE	QyScore	WMH, Atrophy	T1, FLAIR	Brain atrophy per region from T1. Segmentation and volume of WMH from T1 and FLAIR.	AI	FDA (II), CE (IIa)
United Imaging Intelligence	uAI Discover	ICH, ISL, WMH, Atrophy, PVS, Lacunes, CMB, BA	NCCT, CTA, CTP, MRI	Segmentation of ICH, edema, and midline shift from NCCT. ASPECTS score per region from NCCT. Detection of BA from CTA. Segmentation of infarct core and mismatch areas from CTP. Quantitative evaluation of ISL, lacunes, WMH, PVS, CMB, and atrophy from MRI to provide a total CSVD score.	AI	-

3.3. Research systems

Table 3 shows an overview of the 13 research publications identified, with more detail provided in **Table 4**. Only 1 publication focuses on object detection, with the remainder focusing on segmentation. Below we summarise the types of CVD markers and imaging modalities targeted in the publications, the data characteristics, the image analysis methods employed, the validation methods and results, and the risk of bias.

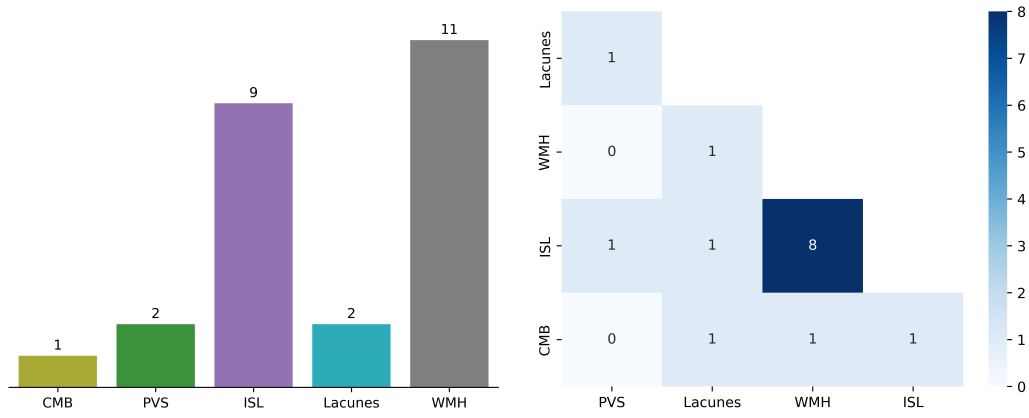
3.3.1. CVD markers and imaging modalities

Some CVD markers were more heavily targeted than others: we see in **Fig 3a** that 11/13 publications dealt with WMH, 9/13 with ISL, 2/13 with PVS, 2/13 with lacunes, and 1/13 with CMB. 3 papers aimed to segment WMH in the presence of ISL (without attempting to segment ISL) ([Shi et al., 2013](#); [Tsai et al., 2014](#); [Liu et al., 2020a](#)). **Fig 3b** shows the co-occurrence of targeted CVD markers within the identified publications. This reveals that the only CVD markers which are targeted jointly more than once are WMH and ISL.

In terms of imaging modalities, **Fig 3d** shows the number of uses of each MRI sequence type to identify (or identify confounders of) each CVD feature. Of the 13 papers, 11 used at least 2 sequences. The only paper to tackle CMB segmentation ([Duan et al., 2020](#)) used T2*, which is essential for identifying these very small bleeds. For tackling PVS, both papers ([Uchiyama et al., 2008](#); [Sudre et al., 2019](#)) used T1 and T2 while the latter additionally used FLAIR. For tackling ISL, the most popular sequences were T1, FLAIR and DWI, with 2 papers also utilising T2. 3 papers exclusively use DWI for ISL identification ([Shi et al., 2013](#); [Tsai et al., 2014](#); [Duan et al., 2020](#)). For tackling lacunes, both [Sudre et al. \(2019\)](#) and [Duan et al. \(2020\)](#) used T1 and FLAIR, with the former also using T2. For tackling WMH, all papers use FLAIR with some additionally using T1. Overall, FLAIR was used the most times to identify a CVD marker, with 22 usages, T1 was used 14 times, T2 was used 6 times, DWI was used 5 times and T2* and T1-FLAIR were each used only once.

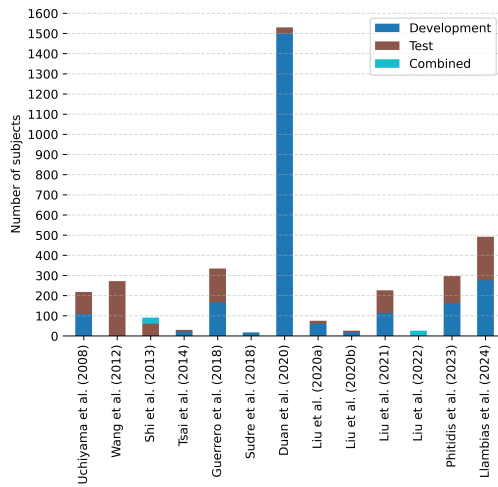
3.3.2. Sample characteristics

Data acquisition. Non-open source data was used by 10/13 papers. The remaining 3 studies ([Liu et al., 2020a,b](#); [Llambias et al., 2024](#)), used publicly

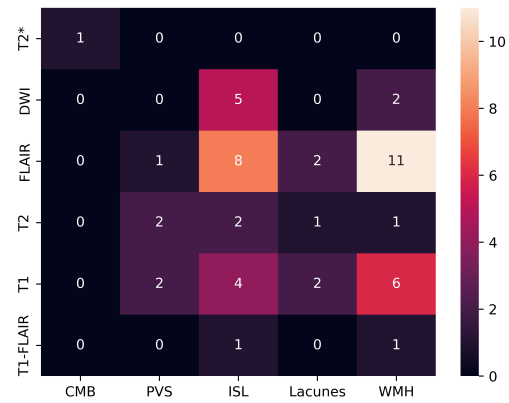


(a) Number of publications targeting each pathology

(b) Co-occurrence of pathologies targeted



(c) Dataset size



(d) Number of uses of each modality for each pathology

Figure 3: Pathology, modality and sample size characteristics of identified research publications.

available data from the WMH segmentation challenge² (Kuijf et al., 2019), the ISLES challenge³ (Hernandez Petzsche et al., 2022), the MSSEG challenge (Commowick et al., 2021), and the MS08 challenge (Styner et al., 2008). Liu et al. (2020a) and Liu et al. (2020b) added additional lesion annotations of their own.

Reference standard. In 7/13 studies, multiple expert annotators generated or endorsed the ground truth (Wang et al., 2012; Sudre et al., 2019; Duan et al., 2020; Liu et al., 2020a,b, 2021, 2022), with the remaining 6/13 studies using annotations generated by a single expert. Most studies used manually generated ground truth, however 3/13 studies state that the ground truth was semi-automatically generated (Tsai et al., 2014; Guerrero et al., 2018; Phitidis et al., 2023). All identified publications except Llambias et al. (2024) utilised data where, for at least some subjects, multiple CVD features are visible within the same image.

Demographics. Only 5/13 papers (Wang et al., 2012; Shi et al., 2013; Tsai et al., 2014; Liu et al., 2021; Phitidis et al., 2023) provided explicit information regarding the mean age and sex of the subjects in their dataset. The mean age ranged from 52 to 70 and comprised a total of 466 male and 337 female subjects.

Data splits. Data splits into development/training and test sets can be seen in **Fig 3c**. In cases where K-fold cross validation was used, the development and test sets are considered to be the total dataset size. For methods which do not use machine learning, 2/3 clearly utilise an independent test set (Shi et al., 2013; Tsai et al., 2014), whilst Wang et al. (2012) do not specify their development data, only their test data. 6/10 machine learning approaches (Uchiyama et al., 2008; Guerrero et al., 2018; Sudre et al., 2019; Duan et al., 2020; Liu et al., 2020a,b; Phitidis et al., 2023; Llambias et al., 2024) utilise a separate test set and 3/10 perform K-fold cross validation (Uchiyama et al., 2008; Guerrero et al., 2018; Liu et al., 2021). Liu et al. (2022) do not make clear the train/test split used. With the exception of (Duan et al., 2020), no publications use more than 297 subjects in total, for development and testing.

²<https://wmh.isi.uu.nl/>

³<https://isles22.grand-challenge.org/>

3.3.3. Preprocessing

To handle the variation in appearance between scans acquired from different scanners, different imaging protocols, and different subjects, some preprocessing is usually performed to normalise the data before running the core image analysis detection/segmentation algorithm. In machine learning, preprocessing is easily defined: it comprises the steps taken before inputs are passed into the machine learning model. These steps should be performed in the same way for the training and testing data. For analytical methods which rely entirely on rules-based processing, it can be more difficult to identify where preprocessing ends and the algorithm begins. In this review, we consider preprocessing to be conventional steps which could feasibly be applied prior to any image processing algorithm, such as registration to a standard template, or normalisation. We consider, for example, more complex tasks like unsupervised brain tissue segmentation as part of the method, not the preprocessing.

Liu et al. (2020a), Liu et al. (2020b), and Llambias et al. (2024) use publicly available datasets, without applying any further preprocessing. We now describe the preprocessing steps taken in the remaining 9 publications (Uchiyama et al. (2008) do not mention preprocessing), making use of non-open source data.

Bias field correction. Bias field correction was applied by 4/9 papers (Wang et al., 2012; Sudre et al., 2019; Liu et al., 2022; Phitidis et al., 2023). Wang et al. (2012) specified the method as non-parametric non-uniform intensity normalisation (Sled et al., 1998) and Liu et al. (2022) used a variant proposed in Tustison et al. (2010).

Coregistration. Coregistration of multiple sequences is stated by 5/9 (Wang et al., 2012; Shi et al., 2013; Tsai et al., 2014; Guerrero et al., 2018; Liu et al., 2022). Of these 5 papers, 2 (Wang et al., 2012; Guerrero et al., 2018) specify the use of FSL-FLIRT⁴ (Jenkinson and Smith, 2001; Jenkinson et al., 2002) as the software used to perform affine registration. Additionally, 1 paper specifies the transformation as affine (Shi et al., 2013) and 1 specifies rigid (Tsai et al., 2014). It should be noted that rigid transformation is a subset of affine transformation for which scaling and shearing is not allowed. The cost function is specified as normalised mutual information (Maes et al., 1997) by

⁴<https://fsl.fmrib.ox.ac.uk/fsl/fslwiki/FLIRT>

2 papers (Shi et al., 2013; Tsai et al., 2014) and as cross-correlation by Wang et al. (2012). None specify the optimisation algorithm or the interpolation method.

Brain extraction. Brain extraction may be equivalently referred to as skull stripping. Brain extraction was reported by 5/9 papers (Wang et al., 2012; Tsai et al., 2014; Sudre et al., 2019; Liu et al., 2022; Phitidis et al., 2023), with the former 2 using FSL-BET⁵ (Smith, 2002) and Liu et al. (2022) using AFNI (Cox, 1996). It may be additionally suspected that Guerrero et al. (2018) performed skull stripping, based on images shown in the paper.

Resampling. Only Guerrero et al. (2018) state that they resample images to a specific spatial resolution (1 mm in the axial plane). Phitidis et al. (2023) utilise nnU-Net (Isensee et al., 2019) for selecting the spatial resolution.

Normalisation. 5/9 papers state that they perform normalisation or standardisation (z-scoring) of voxel intensities (Shi et al., 2013; Tsai et al., 2014; Guerrero et al., 2018; Sudre et al., 2019; Duan et al., 2020). Of these, 3 focused on the white matter region; 1 study (Tsai et al., 2014) scaled the voxels in this region to the range [0,100], 1 study (Sudre et al., 2019) standardised the image using the white matter statistics, and 1 study (Duan et al., 2020) normalised and aligned the histogram peaks based on the white matter region. Guerrero et al. (2018) standardised to the non-background statistics and clipped values below 3 standard deviations from the mean. Shi et al. (2013) simply states that they performed intensity normalisation. Additionally, Liu et al. (2021) perform a gamma transformation on the image patches extracted from the first stage of their solution before passing them to the second stage, in order to stretch the high intensity regions. Phitidis et al. (2023) used the intensity normalisation scheme of nnU-Net.

3.3.4. Rule-based and machine learning methods

The following studies used rules-based (RB) and classical machine learning (ML) methods:

Uchiyama et al. (2008). The authors used the morphological white top-hat transform to enhance hyperintense lesions in the T2 sequences and then applied thresholding to segment the regions of interest. They extracted features

⁵<https://fsl.fmrib.ox.ac.uk/fsl/fslwiki/BET>

including size, shape, location, and difference in T1 and T2 signal intensity. They then used these features to train a 3 layer neural network to classify the segmented lesion as either PVS or lacunar infarct (the result of an ischaemic stroke affecting blood supply to the deep brain tissue). In later work (Uchiyama et al., 2009), they introduced the idea of registering a magnetic resonance angiography (MRA) image to the T1 and T2 images in order to use blood flow to differentiate between lacunar infarcts and PVS, although this was not validated.

Wang et al. (2012). Following preprocessing, the authors used Freesurfer⁶ to segment brain tissues from the T1 images and followed this with a combination of image processing and computer vision techniques on the T1, T2 and FLAIR scans. For instance, they fit Gaussian mixture models (GMMs) to identify relevant tissue thresholds prior to thresholding, then apply morphological operations of erosion, dilation and region growing.

Shi et al. (2013). The authors segmented WMH in the presence of acute infarcts. Following preprocessing, they fused the T1 and FLAIR images and from this segmented white matter, grey matter and cerebrospinal fluid. To identify the WMH they focused on FLAIR and performed: grayscale morphological closing followed by a local standard deviation operation to identify borders of hyperintense regions; thresholding; binary morphological dilation; grayscale morphological reconstruction within the mask area; thresholding the difference image between the original FLAIR and reconstructed image; and finally binary morphological reconstruction. Infarcts were detected in DWI using thresholding, dilation, and morphological reconstruction and then subtracted from the final WMH segmentation.

Tsai et al. (2014). Following preprocessing, the authors developed a scheme based on fusion of T1 and FLAIR images. Probabilistic white and grey matter masks were generated using the New Segment module of SPM8⁷ on the fused image and a brain template (ICBM), and these were used to estimate the registration between the images with the DARTEL module of SPM8. In the same space, a logical AND operation was performed between appropriate template labels and the binarised probabilistic white matter mask of

⁶<https://surfer.nmr.mgh.harvard.edu/>

⁷<https://www.fil.ion.ucl.ac.uk/spm/>

the image, resulting in the final white matter mask. The FLAIR image was normalised within this region and thresholded to located candidate WMH. A mask of the grey/white matter junction was generated from the fused image and WMH which significantly overlapped with this mask were eliminated. Finally ISL were detected by thresholding the DWI image and WMH overalpping these were eliminated also.

3.3.5. Deep learning methods

A summary of the design choices made by the methods that used DL can be seen in **Table 2**. Some common themes are the use of CNNs, cross-entropy or Dice loss, batch normalisation, and the ReLu activation function. The following studies used DL:

Guerrero et al. (2018). The authors implemented a 2D CNN based on the successful U-Net architecture (*Ronneberger et al., 2015*), which they termed uResNet. Their main enhancement of the standard U-Net model was introducing residual connections (*He et al., 2016*) within each layer.

Sudre et al. (2019). A 3D model based on RCNN (*Girshick et al., 2014*) was developed by the authors to detect lacunes and PVS. They do not resize or pool the selected bounding box regions as is done in the original framework, since the target objects (lacunes and PVS) are small making them prone to distortion during resizing, likely leading to worse model performance. Their model attempts to classify each region as nothing, lacune, PVS, or either lacune or PVS.

Duan et al. (2020). The authors used 4 independently trained 2D U-Nets to segment WMH, lacunes, infarcts, and microbleeds from different sequences as detailed in **Table 4**.

Liu et al. (2020a). The authors developed a 2D CNN method which they coined M2DCNN. The model utilised 2 symmetric U-Net-like networks at different resolutions to extract multi-scale features. At the encoder-decoder bottlenecks they employed dilated convolutions with a stride of 1 to enlarge the receptive field size whilst maintaining the same feature map dimensions. They also replaced the standard convolution blocks with dense blocks (*Huang et al., 2017*).

Liu et al. (2020b). A 2D U-Net model was developed by the authors, termed DRANet, incorporating an attention block acting on the residual features. This block has 2 internal branches, comprising the trunk branch which is made up of residual blocks and the dilated soft mask branch which incorporates dilated convolutions and ends with a sigmoid activation. The output of the two branches are then summed element-wise. The authors claim that since the inputs to the trunk and soft mask branches are the same, then the soft mask branch will either construct the identity mapping to reinforce the residual features, or contribute new features to suppress noise which may be present.

Liu et al. (2021). The authors implemented a two stage approach for segmenting small focal cerebral ischaemia and lacunar infarcts. The first stage utilised T2-FLAIR input to a 2D U-Net producing a binary mask to differentiate foreground lesions from background. For each predicted foreground connected component, a 32×32 crop of the corresponding T1-FLAIR images was taken about its centroid and used as input to a CNN which classified the lesion.

Liu et al. (2022). The authors modify a 2D U-Net to include a global branch utilising transformer layers. The self attention mechanism working on flattened image patches allows long-range features to be learned with even a single layer, which is not the case for convolution. The features are incorporated at the bottleneck of the U-Net.

Phitidis et al. (2023). In this work, the authors evaluated two existing self-configuring, out-of-the-box segmentation frameworks: nnU-Net ([Isensee et al., 2021](#)), and Auto3DSeg⁸ ([MONAI Consortium et al., 2020](#)), for the WMH and ISL segmentation task, from FLAIR images.

Llambias et al. (2024). The authors trained a model to segment WMH, ISL, and MS lesions using separate, partially labelled datasets. They initially trained a 2D U-Net model on all the datasets to perform binary lesion segmentation. Then, they fine-tuned the model to perform multiclass segmentation, using a weighted sampling strategy to ensure an equal number of slices with each pathology. Then, they further fine-tuned the model, using the same sampling strategy, but reverting back to the binary segmentation setting. To

⁸<https://monai.io/apps/auto3dseg>

Table 2: Deep learning system design choices for included publications.

Study	Pre ¹	Arch ²	Post ³	Aug ⁴	Loss ⁵	Dim	Dil	Norm ⁶	Act	Drop	MS	LR	Ens
Guerrero et al. (2018)	K,R,S	uResNet		F	CE	2D		B	ReLu			✓	
Sudre et al. (2019)	B,K,S	RCNN			CE, RMSE	3D	✓	B	ReLu				
Duan et al. (2020)	H	U-Net	R			2D							✓
Liu et al. (2020a)		M2DCNN			D*	2D	✓	B	ReLu	✓	✓		
Liu et al. (2020b)		DRANet			D	2D	✓			✓	✓		
Liu et al. (2021)		U-Net, CNN		R	CE	2D		B	ReLu	Y			✓
Liu et al. (2022)	B,K,R	LLRHNNet			D	2D		L	ReLu	✓	✓		
Llambias et al. (2024)		U-Net, FCN		F,R, E,N, B,M	D, CE	2D						✓	✓

1. Preprocessing: B = bias field correction, H = histogram based normalisation, K = skull stripping, N = normalisation (scaling), R = resampling, S = standardisation (z-score), T = transformation to template (e.g. NMI).

2. Architecture.

3. Postprocessing: R = mask subtraction rules.

4. Augmentation: F = flipping, R = rotation, E = elastic, N = noise, B = bias field, M = motion artefacts.

5. Loss function: CE = cross-entropy, D = Dice, RMSE: root mean square error.

6. Normalisation: B = batch, I = instance, L = Layer.

Act: activation function, Dim: dimension of convolutions, Dil: use of dilated convolutions, Drop: use of dropout, MS: use of multi-scale features (processed separately), LR: use of learning rate scheduler, Ens: ensemble of models.

Note: Phitidis et al. (2023) not included since the authors use existing frameworks.

* Variant of standard dice loss where the function is: $1 - \text{lesion_dice_score} - \text{background_dice_score}$

classify the lesion type, they trained a fully connected network (FCN) on manually extracted features of each connected component. These features were the volume, surface area, orientation, and principle axis length.

3.3.6. Validation

From **Fig 3c** it can be seen that of the papers which gave information regarding their development and testing data splits (Uchiyama et al., 2008; Shi et al., 2013; Tsai et al., 2014; Guerrero et al., 2018; Sudre et al., 2019; Duan et al., 2020; Liu et al., 2020a,b, 2021; Phitidis et al., 2023; Llambias et al., 2024), 5/10 studies (Uchiyama et al., 2008; Shi et al., 2013; Tsai et al., 2014; Guerrero et al., 2018) utilised at least 50% of their total data for testing. Notably, Duan et al. (2020) used only 30 cases (with 2-4 CVD markers) for testing, despite the comparatively large amount of training data.

White matter hyperintensities. Of the 10 papers which perform WMH segmentation and provide a DSC, 9 provide the standard deviation of the DSC (or a box plot from which we have estimated it). These results are shown in **Fig 4a**, where it can be seen that the average reported mean value for this subset is 0.76 and the lowest is 0.691. Not included in the plot, Duan et al. (2020) report 0.666. It should be emphasised that these studies used different datasets and so direct comparison of the scores achieved has limited

value.

Ischaemic stroke lesions. Out of 9 papers tackling ISL segmentation, 7 stated a DSC and 5 presented the standard deviation of the DSC (or a box plot from which we have estimated it). The reported mean DSC in this subset averages 0.59, but there is a wide range in results (0.324 to 0.791), indicating unreliable performance, but also potentially variation caused by different task settings (subcortical or cortical strokes, presence of WMH, use of DWI, etc). [Duan et al. \(2020\)](#), which is not included in the plot, reported a mean DSC of 0.728 for subcortical ISL which they segment in DWI images. [Uchiyama et al. \(2008\)](#) did not report an overlap metric, but classify ISL versus PVS with an AUC of 0.945. However, they stated a specificity of only 0.75, which may be due to the class imbalance present in their training data (89 ISL versus 20 PVS instances). [Liu et al. \(2021\)](#) provide an overlap metric for foreground (WMH or ISL) vs background, achieving a DSC of 0.742.

Enlarged perivascular spaces. Of the 2 papers considering PVS detection, neither provided the DSC. [Uchiyama et al. \(2008\)](#) did not provide any metrics for PVS, since their goal was to differentiate ISL from PVS. [Sudre et al. \(2019\)](#) proposed a model for detecting small objects including lacunes and PVS, but after detecting some uncertainties in their test cases, focused the validation instead on the overall sensitivity of their model to these small objects (0.727) and the median predicted bounding box overlap (59%).

Lacunes. Of the 2 methods concerned with the identification of lacunes, 1 provided their DSC to be 0.496 ([Duan et al., 2020](#)) whilst the other only provided small object sensitivity and bounding box overlap as described above ([Sudre et al., 2019](#)).

Cerebral microbleeds. Only [Duan et al. \(2020\)](#) attempt CMB segmentation; they use T2* MRI and achieve a DSC of 0.503.

3.3.7. Risk of bias and applicability

The results of the analysis of the risk of bias and applicability can be seen in **Table 5**.

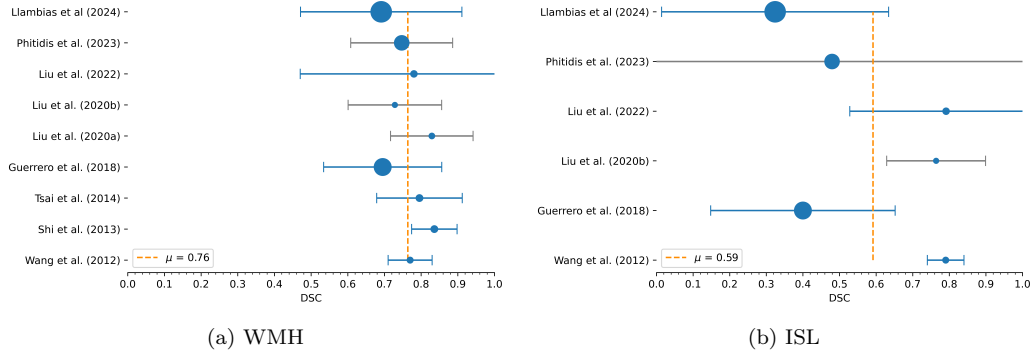


Figure 4: Reported Dice similarity coefficients (DSC) for WMH and ISL. Error bars are standard deviation and marker size corresponds to test dataset size. Grey error bars indicated that the standard deviation was not reported and has been estimated visually from box plots as 3/4 of the interquartile range (assumes normal distribution).

Table 3: Identified research publications - high-level overview.

Study	Pathology	Modality	Features	Method class
Uchiyama et al. (2008)	ISL, PVS	T1, T2	Segmentation of lacunar infarcts and PVS	RB, ML
Wang et al. (2012)	WMH, ISL	T1, T2, FLAIR	Segmentation of WMH and cortical and lacunar infarcts	RB
Shi et al. (2013)	WMH	T1, FLAIR, DWI	Segmentation of WMH in the presence of ISL	RB
Tsai et al. (2014)	WMH	T1, FLAIR, DWI	Segmentation of WMH in the presence of ISL	RB
Guerrero et al. (2018)	WMH, ISL	T1, FLAIR	Segmentation of WMH and ISL	DL
Sudre et al. (2019)	Lacunes, PVS	T1, T2, FLAIR	Detection of lacunes and PVS	DL
Duan et al. (2020)	WMH, ISL, lacunes, CMB	T1, T2*, FLAIR, DWI	Segmentation of WMH, subcortical infarcts, lacunes and CMB	DL
Liu et al. (2020a)	WMH	T1, FLAIR	Segmentation of WMH in the presence of ISL	DL
Liu et al. (2020b)	WMH, ISL	FLAIR, DWI	Segmentation of WMH and ISL	DL
Liu et al. (2021)	WMH, ISL	FLAIR, T1-FLAIR	Segmentation of small WMH and ISL	DL
Liu et al. (2022)	WMH, ISL	FLAIR, DWI	Segmentation of WMH and ISL	DL
Phitidis et al. (2023)	WMH, ISL	FLAIR	Segmentation of WMH and ISL	DL
Llambias et al. (2024)	WMH, ISL	FLAIR	Segmentation of WMH and ISL	DL

Pathologies:

ISL: ischaemic stroke lesions, PVS: enlarged perivascular spaces, WMH: white matter hyperintensities, CMB: cerebral microbleeds.

Modalities:

T1: T1-weighted MRI, T2: T2-weighted MRI, FLAIR: fluid-attenuated inversion recovery MRI, DWI: diffusion-weighted imaging MRI, T2*: T2-weighted MRI.

Other abbreviations:

RB: rule-based, ML: machine learning, DL: deep learning.

Table 4: Identified research publications - study details.

Pathologies:

PVS: enlarged perivascular spaces, WMH: white matter hyperintensities, ISL: ischaemic stroke lesions, CMB: cerebral microbleeds.

Modalities:

T1: T1-weighted MRI, T2: T2-weighted MRI, T2*: T2*-weighted MRI, FLAIR: fluid-attenuated inversion recovery MRI, DWI: diffusion-weighted imaging MRI.

Metrics:

AUC: area under the receiver operating characteristic curve, Sen: sensitivity, Spe: specificity, Pre: precision, DSC: Dice similarity coefficient, r: Pearson's correlation coefficient, TP: true positive, slope: gradient of linear fit of prediction with ground truth volume, R²: coefficient of determination, IIC: intraclass correlation coefficient, HD: Hausdorff distance, Acc: accuracy, Rec: recall, RMSE: root mean square error, F1: DSC at lesion level with at least one true positive voxel classing the prediction as a true positive.

Study	Population	Reference standard	Preprocessing	Training	Validation
Uchiyama et al. (2008)	109 patients with 89 lacunar infarcts and 20 PVS.	Lesion-wise labels from experienced radiologist.	Not stated.	Leave one out method.	AUC = 0.945, Sen = 0.933, Spe = 0.75 (for lacunar infarcts)
Wang et al. (2012)	272 subjects from an ageing cohort (70 ± 6.3 years, 131 male, 141 female).	WMH and cortical infarcts manually delineated in 19 subjects by two trained clinicians under guidance of a neuroradiologist and lacunar infarcts manually delineated by clinician on all 272 subjects. ITK-SNAP used and all modalities utilised. ARWMC visual score rated by two trained clinicians.	Bias field correction, affine registration of T2 and FLAIR to T1 with cross correlation as cost function, skull stripping of FLAIR image using BET.	N/A	WMH: DSC = 0.77, r = 0.728 with ARWMC. Cortical infarct: DSC = 0.79. Lacunar infarct: Sen (>= 1 TP) = 0.86, Pre (>=1 TP) = 0.74.
Shi et al. (2013)	91 subjects with acute infarction (64.43 ± 10.54 years, 65 male, 26 female).	WMH manually delineated on 30/91 subjects by experienced neuro-radiologist using ITK-SNAP. Qualitative scores by experienced neuro-radiologist using ARWMC for all 91 subjects.	T1 and DWI affinely registered to FLAIR using normalised mutual information and then intensity normalised.	N/A	DSC = 0.836, Sen = 0.803, Pre = 0.818, Slope = 0.9967, IIC = 0.9892, Vol (quadratic) fit R = 0.8442.
Tsai et al. (2014)	30 subjects with acute ischaemic stroke. Derivation subset: 20 subjects, 69.9 ± 12.2 years, 12 male, 8 female. Validation subset: 10 subjects, 63.4 ± 11.9 years, 7 male, 3 female.	WMH semi-automatically derived by neurologist.	T1 and DWI rigidly registered to FLAIR image using normalised mutual information and DWI skull stripped. FLAIR normalised within white matter region.	N/A	Hemisphere-wise. Derivation: WMH only: DSC = 0.8314, Sen = 0.8415, Spe = 0.9999, Slope = 0.707, R ² = 0.848, ICC = 0.905. WMH and stroke: DSC = 0.6883, Sen = 0.7438, Spe = 0.9996, Slope = 1.021, R ² = 0.676, ICC = 0.784. Validation: WMH only: DSC = 0.8321, Sen = 0.8152, Spe = 0.9991, WMH and stroke: DSC = 0.7646, Sen = 0.7614, Spe = 0.9999.

Guerrero et al. (2018)	167 subjects from studies of non-disabling stroke.	83 subjects WMH were segmented using MCMxxxVI. 84 subjects WMH were segmented semi-automatically using human corrected histogram thresholding from FLAIR. Strokes segmented semi-automatically by thresholding and region growing guided by domain knowledge.	Registration to FLAIR space using FSL-FLIRT (reference, date), in-plane resampling to 1 mm and intensity standardisation with voxels below three standard deviations from the mean clipped.	Patch size of 64x64 pixels with centre shifting so a foreground class is not always in the centre, batch size of 128, cross entropy loss, Adam optimiser with learning rate 0.0005, 30 epochs.	WMH: DSC = 0.695, Slope = 0.89, R ² = 0.951, r (Fazekas) = 0.824. Stroke lesions: DSC = 0.4, Slope = 0.58, R ² = 0.791.
Sudre et al. (2019)	16 subjects from a tri-ethnic cohort with elevated vascular burden (14 train, 2 test).	Manual segmentation of lacunes and PVS using three available sequences using ITK-SNAP followed by removal of infeasible voxels or components with volume less than 5 voxels. Each component was independently classified by six raters as: 1) nothing 2) lacune 3) PVS 4) lacune or PVS.	Coregistration (assumed), bias field correction, skull stripping, standardised to white matter region statistics.	Backbone trained first, then region proposal network, then classification network. Patch size of 64x64x64 sampled according to inverse weighted distance from a foreground class. RMSE, cross entropy and custom distance loss used.	Sen = 0.727, Median box overlap (where all raters agreed) = 59%.
Duan et al. (2020)	Training data of 1500 subjects with ischaemic stroke or TIA from 12 hospitals resulting in a total of 824 T1 and FLAIR images from 824 subjects with lacunes or WMH, 1010 DWI images from 1010 subjects with subcortical infarcts, and 359 T2* images from 359 subjects with cerebral microbleeds. Evaluation dataset of 30 subjects with 2-4 signs of SVD.	Training data segmentations endorsed by two radiologists with 12 years clinical experience - lacune labels on T1 with reference to FLAIR, WMH on FLAIR, subcortical infarct on DWI, and cerebral microbleed on T2*. Evaluation segmentations on consensus of three senior physicians with 12, 13 and 15 years experience.	Coregistration (assumed), histogram peaks normalised and aligned based on white matter .	One network per SVD feature with FLAIR input for WMH and lacunes, DWI for infarcts and T2* for microbleeds. Training is stopped when training accuracy is greater than 98% and diverged from validation accuracy by more than 15%.	WMH: DSC (voxel) = 0.666, DSC (lesion) = 0.644. Subcortical infarct: DSC (voxel) = 0.728, DSC (lesion) = 0.859. Lacunes: DSC (voxel) = 0.496, DSC (lesion) = 0.683. CMB: DSC (voxel) = 0.503, DSC (lesion) = 0.713.
Liu et al. (2020a)	Training data of 60 (52 training, 8 validation) images from the WMH segmentation challenge (25 with stroke lesions). Testing data of 15 cases from the ISLES challenge, all with WMH also.	Segmentations of WMH in training data provided by challenge organisers and segmentation of stroke in test data also provided by challenge organisers while segmentation of WMH in test data were manually segmented from FLAIR by two experienced clinicians using ITK-SNAP.	Not stated.	Trained for 150 epochs with batch size 3 using Adam optimiser with learning rate 0.001, drop out of 0.3 and early stopping if the training loss does not change for 10 epochs.	WMH only: DSC = 0.8354, HD = 2.29. WMH and stroke: DSC = 0.8227, HD = 2.2. DSC (WMH on stroke) = 0.0069. Stroke only: DSC (WMH on stroke) = 0.0265. No lesions: FP = 1/28.

Liu et al. (2020b)	26 subjects with sub-acute ischaemic stroke from the ISLES challenge. 566 train, 52 val, 224 test slices.	Stroke lesion segmentation provided by challenge organisers and WMH segmentation performed by two experienced radiologists on FLAIR using ITK-SNAP.	Not stated.	Trained for 150 epochs with batch size 3 using Adam optimiser with learning rate 0.0001 and dropout rate 0.01.	WMH: DSC = 0.7283. HD = 2.63. Stroke: DSC = 0.7639. HD = 3.19. Image level: Acc = 94.04. Rec = 94.4.
Liu et al. (2021)	113 clinical patients. 61 male, 52 female, 52 ± 26 years, single scanner, 68, 30, and 37 with WMH, ISL, and healthy respect. 5-fold cross validation.	Manual labelling by two experienced radiologists.	Not stated.	FLAIR input to U-Net for stage one binary prediction. Prediction and T1-FLAIR as input to second CNN to classify as WMH/ISL. 5-fold cross-validation. Foreground lesion over-sampling. Cross-entropy loss and RMSProp with moving average weight 0.9 and base learning rate 0.01, drop out layers.	DSC = 0.7421 (foreground vs background), Pre = 0.9176 (detection of foreground). Pre = 0.9289 (classification of lesion). True positive if IoU > 0.6.
Liu et al. (2022)	26 subjects with both WMH and ISL (468 images slices). Single scanner, 20-50 years.	Semi-automatic labelling by two experienced radiologists. Gold standard based on DWI.	Skull stripping, coregistration, and bias field correction.	80 epochs, dice loss, batch size 3, learning rate 0.001, drop out rate 0.3.	WMH: DSC = 0.7802 ± 3.1, HD = 2.27 ± 2.01, ISL: DSC = 0.791 ± 2.63, HD = 2.70 ± 1.51
Phitidis et al. (2023)	297 subjects with SVD from 4 diverse imaging protocols. 64% male, 67 ± 11 years, 20% diabetes, 70% hypertension, 54% current or ex smokers. 131 cortical ISL, 133 sub-cortical ISL, 10 both, 23 without ISL. 162 train and 135 test, stratified by ISL subtypes.	Expert ISL segmentation and semi-automatic WMH with expert correction.	Skull stripping and bias field correction followed by nnU-Net and Auto3DSeg specific pre-processing.	nnU-Net and Auto3DSeg specific.	(nnU-Net) WMH: DSC = 0.7469, Pre = 0.7745, Rec = 0.7506, HD95 = 10.16 ISL: DSC = 0.4795, Pre = 0.6520, Rec = 0.4278, HD95 = 30.21

<p>Llambias et al. (2024)</p>	<p>combination of 4 public datasets for MS, WMH and ISL segmentation: MSSEG-1, MS08, ISLES22, WMH challenge dataset. 276 train, 216 test.</p>	<p>Segmentations provided by challenge organisers.</p>	<p>Not stated.</p>	<p>2D U-Net trained in stages. First trained to segment foreground vs background. Next fine-tuned for multiclass segmentation of MS, ISL, and WMH with equally weighted sampler. Next fine-tuned for foreground vs background again, using equally weighted sampler. An FCN is trained to classify each connected component based on extracted features. For the U-Net: 250k batches, batch size 64, cosine annealing with initial learning rate 0.001, SGD, Dice + cross-entropy loss. For the FCN: 2 layers with 400 nodes, weighted cross-entropy, Adam with learning rate 0.1, 100 epochs. Augmentation: Generic spatial and intensity, bias field simulation, motion artefacts simulation.</p>	<p>(Cascade model) WMH: DSC = 0.691 ± 0.22, F1 = 0.686 ± 0.21, ISL: DSC = 0.324 ± 0.31, F1 = 0.335 ± 0.26</p>
-------------------------------	--	--	--------------------	---	--

4. Discussion

Preponderance of solutions for single rather than multiple CVD markers. Many solutions for CVD marker identification were excluded due to our inclusion criteria of requiring *multiple* CVD markers to be tackled. For instance, all research on ICH and/or LVO was excluded from this review (e.g. the

Table 5: Risk of bias assessment of the studies reviewed using the QUADAS 2 tool.

STUDY	RISK OF BIAS					APPLICABILITY			
	PATIENT SELECTION	INDEX TEST	REFERENCE TEST		FLOW & TIMING	PATIENT SELECTION	INDEX TEST	REFERENCE TEST	
	Could the selection of patients have introduced bias?	Could the method have introduced bias?	Is the ref. std. likely to be correct?	Is the ref. std. manipulated blind to the index test?	Did all data have the same ref. std.?	Were all subjects included?	Do the included patients match the review questions?	Are there concerns about applicability?	Are there concerns about reproducibility?
Uchiyama et al 2008	Medium	Bad	Medium	Medium	Good	Good	Good	Good	Bad
Wang et al 2012	Medium	Good	Good	Bad	Good	Bad	Good	Good	Good
Shi et al 2013	Medium	Good	Good	Bad	Good	Bad	Good	Good	Good
Tsai et al 2014	Good	Bad	Bad	Medium	Good	Bad	Good	Good	Good
Guererro et al 2018	Good	Good	Good	Medium	Good	Medium	Bad	Good	Good
Sudre et al 2019	Good	Good	Good	Medium	Good	Good	Good	Good	Good
Duan et al 2020	Good	Bad	Good	Good	Medium	Medium	Good	Good	Bad
Liu et al 2020 (a)	Good	Good	Good	Medium	Medium	Good	Good	Good	Bad
Liu et al 2020 (b)	Good	Good	Good	Medium	Good	Good	Good	Good	Bad
Liu et al 2021	Good	Bad	Good	OK	Good	Good	OK	OK	Good
Liu et al 2022	Bad	Good	OK	OK	Good	Bad	OK	Good	Bad
Phitidis et al 2023	Good	Good	OK	Good	OK	Good	Good	Good	Good
Llambias et al 2024	Good	Good	Good	Good	OK	Good	Good	Good	OK

work by Wang et al. (2021) for the RSNA ICH detection kaggle challenge⁹ (Flanders et al., 2020)). Many of these research methods were stimulated by challenges such as ISLES which focus on single pathologies. It would be interesting to see these methods applied to the more holistic CVD assessment that we consider in this review. Unfortunately, research in this area has been hampered by a lack of publicly available datasets with multiple CVD markers present and labelled by experts. Further, with the exception of Enterprise CTB, no other commercial systems claim to identify PVS or CMB and none identify lacunes. These are important markers for the assessment and management of CVD and the ability to automated their detection and quantification would provide a great benefit.

Vulnerability of commercial solutions to chronic ISL. WMH and subacute or chronic ISL have similar appearance in most MRI sequences; they can be difficult to differentiate and may co-occur in the same patient. Only two commercial solution jointly considered the detection of WMH and ISL. One is icobrain, although this is via independent subsystems intended for use in different situations: an acute stroke segmentation system requiring CTP; and a WMH segmentation system requiring T1-weighted and FLAIR MRI sequences. The other is uAI Discover CSVD, although sufficient information was not found for this product; other than this, no commercial systems considered chronic ISL. There were various research publications tackling

⁹<https://www.kaggle.com/c/rsna-intracranial-hemorrhage-detection>

this difficult problem.

Lack of publicly available data for CVD markers. We already mentioned that most public datasets focus on a single pathology e.g. ISLES or the RSNA ICH detection kaggle challenge. To the best of our knowledge, until the recent “Where is VALDO” challenge (Sudre et al., 2023), there were no public datasets with annotations for lacunes, PVS or CMB, even individually. This holds back progress toward the development of a complete CVD support system and points to a lack of awareness surrounding the importance of these imaging markers in CVD assessment, compared to WMH, ISL, and ICH.

Lack of commercial solutions for MRI in acute stroke. It is unsurprising that the acute stroke systems almost all use NCCT, since thanks to its speed and accessibility, it is the most widely used imaging modality. However, DWI has been shown to be more sensitive to acute ischaemic changes (Lansberg et al., 2000). Therefore, DWI may see more uptake in the future and so systems to identify ISL using DWI may be highly desirable if this does happen. For the general neuroradiology support systems on the other hand, we see MRI being used exclusively. T1-weighted is mostly used for brain region segmentation due to its high level of detail and contrast between tissues, while FLAIR is most often utilised for identifying WMH, because it offers superior contrast between these features and surrounding tissue.

Bias towards male subjects. Of the 5 research papers which reported the sex of subjects, 4 used data with a bias towards male subjects, which may have introduced bias in the algorithms. Additional evaluation on female patients would be valuable to understand the performance of the proposed methods. It should be noted that these are small sample sizes and hence finding biases is expected.

Lack of methodological transparency and reproducibility. In terms of risk of bias, the most entries labelled as “bad” in **Table 5** were in the columns headed “Were all subjects included?” and “Are there concerns about reproducibility?”. These were mainly due to unexplained filtering of the available data and insufficient detail to reproduce the method, respectively. A lack of standardised benchmark datasets renders the meaningful comparison of metrics between methods impossible, further inhibiting transparency and reproducibility.

Popularity of convolutional neural networks. Of the subsystems with information on the method, 95% of commercial stroke subsystems and 62% of general commercial neuroradiology support subsystems employ DL. While transformers (Vaswani et al., 2017) are the most widely used architecture in natural language processing today, CNNs still dominate medical image analysis. This may be because their inductive biases (spatial invariance and locality) - while limiting their potential to model global context - allow them to learn more readily from limited data, which is important in the medical domain. Of the DL methods identified in this review, only one single product utilises a VIT architecture (Enterprise CTB); this is facilitated by a training dataset of 200,000 images.

The oldest four research publications use rule-based methods and/or classical machine learning techniques, while the most recent nine all use DL. This highlights a shift in researchers' methods of choice, likely driven by the success of DL in other computer vision applications. All DL based methods identified in this reviews use variations of CNNs, mainly with a U-Net architecture. Again, due to the lack of standardised benchmark datasets, it is not currently possible to say whether this transition to DL has benefited algorithms' performance.

In general, DL provides some obvious benefits as well as some clear drawbacks when compared to other methods. Firstly, once trained, inference is usually very fast. For example, the publicly available DL model SynthSeg (Billot et al., 2023) can perform brain anatomy segmentation in under a minute, whereas the popular Freesurfer tool fits a model for each new images, meaning that it can take several hours to segment a single scan. ATLAS propagation based segmentation methods also require model fitting at test time to find the optimal transformation. These differences may have a significant impact on product viability, since brain anatomy segmentation is a key stage in many of the identified systems, especially those quantifying brain atrophy. While inference speed is a benefit of using DL models, the hardware required to run them efficiently (GPUs with tens of gigabytes of memory) is expensive. Additionally, training them often requires several days or even weeks of continuous energy usage, which is not environmentally friendly. DL models usually have millions of learnable parameters, which is what gives them their ability to model complex functions. However, this means that they are data hungry, and so large amounts of data are required to train them effectively. Their design also limits their explainability (i.e. our ability to step through and understand the impact of each stage of the computation

on the final prediction). Classical method such as random forests have far less parameters and so they are less prone to overfit the training data when it is limited. We are also able to examine and intuitively understand the nodes of each decision tree. All machine learning based methods depend heavily on the quality and coverage of the training data.

Integration into the clinical workflow. A significant barrier to the adoption of new technologies into the clinical workflow is the potential complexity of systems integration. Whilst this is undoubtedly a challenge, several of the commercial systems identified in this review have shown that it is not an insurmountable one, and that the positive clinical impact of the investment can be substantial (see the “Impact” column in **Table 1** of the supplementary material).

Limitations. Data extraction was performed by a single author (J.P.) following the search strategy. Commercially available software systems are constantly evolving with technology and consumer demand, meaning that the details presented in this systematic review may become outdated.

5. Conclusion

There is at this time no comprehensive, fully automated and well validated neuroradiological support system for all non-acute CVD findings (ISL, WMH, PVS, CMB, lacunes, and atrophy). We propose that such a system would provide a great benefit to society, as CVD is a leading cause of dementia and stroke, and automatic quantification of all of these features would open the door for more large-scale research and more efficient patient management. This could build on the success of acute stroke detection systems which are currently being utilised in several hospitals around the world with a reportedly positive impact on patient care, and software used in clinics to automate the arduous manual process of brain volume estimation and WMH segmentation.

The recent advancements in DL hold promise for the future of automatic evaluation of CVD markers. Further methodological innovations in the areas of data-efficient learning and small lesion segmentation, as well as an increase in the availability of standardised benchmark datasets and metrics (using best practices agreed by the research community (Maier-Hein et al., 2024; Reinke et al., 2024)), will likely be required before development of a complete and robust system is feasible.

CRedit authorship contribution statement

Jesse Phitidis: Conceptualization, Methodology, Data curation, Writing - original draft. **Alison Q O’Neil:** Writing - original draft, Writing - review & editing, Supervision. **William N Whiteley:** Writing - review & editing, Resources, Supervision. **Beatrice Alex:** Writing - review & editing, supervision. **Joanna M. Wardlaw:** Writing - review & editing, Resource, Supervision. **Miguel O. Bernabeu:** Writing - review & editing, Supervision. **Maria Valdés Hernández:** Conceptualization, Methodology, Resources, Writing - original draft, Writing - review & editing, Supervision.

Declaration of competing interests

Alison Q O’Neil and Jesse Phitidis are employed (Alison Q O’Neil) or funded (Jesse Phitidis) by Canon Medical Research Europe - an organisation selling commercial medical imaging software. Canon Medical Research Europe has a partnership with Avicenna.AI.

Acknowledgements

Funding: Medical Research Scotland [ref. PHD-50441-2021]; Canon Medical Research Europe; BHF Data Science Centre (at Health Data Research UK); National Institute of Health research (UK); Alzheimer’s Disease Data Initiative; the Neurii initiative which is a partnership among Eisai Co., Ltd, Gates Ventures, LifeArc and HDR UK; Alzheimer’s Society; The Stroke Association; Legal & General Group via Advanced Care Research Centre at University of Edinburgh; NIHR via the Artificial Intelligence and Multimorbidity: Clustering in Individuals, Space and Clinical Context (AIM-CISC) project [NIHR202639]; The Row Fogo Charitable Trust [Ref No: AD.ROW4.35. BRO-D.FID3668413]; Fondation Leducq Perivascular Spaces in Small Vessel Disease [16 CVD 05]; UK Dementia Research Institute [award no. UKDRI – Edin002, DRIEdi17/18, and MRC MC_PC_17113] which receives its funding from DRI Ltd, funded by the UK Medical Research Council, Alzheimer’s Society and Alzheimer’s Research UK; Stroke Association/BHF/Alzheimer’s Society ‘Rates Risks and Routes to Reduce Vascular Dementia’ (R4VaD) Priority Programme Award in Vascular Dementia [16 VAD 07] ; British Heart Foundation Centre for Research Excellence Award III [RE/18/5/34216]; British Heart Foundation and The Alan Turing Institute Cardiovascular Data Science Award [C-10180357]; Dementias Platform

UK 2 – Integrated Dementia Experimental Medicine. UK Medical Research Council; [MR/T033371/1]; The Galen and Hilary Weston Foundation [ref UB190097]; Fondation Leducq Transatlantic Network of Excellence [17 CVD 03]; EPSRC [grant no. EP/X025705/1]; Diabetes UK [20/0006221]; Fight for Sight [5137/5138]; the SCONE projects funded by Chief Scientist Office, Edinburgh & Lothians Health Foundation, Sight Scotland, the Royal College of Surgeons of Edinburgh, the RS Macdonald Charitable Trust, and Fight For Sight.

Appendix A. Supplementary Material

For commercial systems, detailed information on the methods and training data were mostly not available through the websites, whitepapers, explicitly cited publications, or FDA premarket notifications. Since this is a particular point of interest, we additionally looked at: a) the linked publications on the website; and b) the first page of results for a Google Scholar search of the form *company AND sub-product AND pathology*. It should be noted that as commercial software, algorithms and training data are likely to continuously evolve and so where possible, the most recent information is referenced.

Table A.6: Commercial systems - details. With the exception of methods and training data (which were identified via linked publications or independent search where required and possible), the entries in this table are from the company website, whitepapers, explicitly cited publications, or FDA premarket notifications. Where these have not provided information, this has been stated, and where there are multiple sources of validation results, the most detailed has been presented. Linked publications are publications linked on the company website or in brochures, but not necessarily explicitly cited.

Product	(sub-product) Population	(Sub-product) Reference standard	(sub-product) Method/Training	(sub-product) Validation	(sub-product) Impact	Linked publications
Always-on AI	<p>(BriefCase ICH) Training: ~50,000 cases from 9 sites and 17 different scanners (63). Validation: 3 sites (2 in USA), 198 cases (~50% with ICH) (1).</p> <p>(BriefCase LVO) Validation: 3 sites in USA, 383 cases with LVO (2).</p> <p>(BriefCase BA) Validation: 5 sites, multinational, 286 cases (96 with BA) (3).</p> <p>(icobrain-cva) Validation: A clinical dataset and digital phantom (4).</p>	<p>(BriefCase BA) Validation: Ground thruth generated by 2 US board-certified radio- logists with a third in case of disagreement (3).</p>	<p>(BriefCase ICH) 3D CNN proposes regions and second stage filters based on final layer features (64).</p> <p>(BriefCase LVO) CNN (65).</p> <p>(icobrain-cva) CNN trained to predict AIF by optimising lesion segmentation objective (7).</p>	<p>(BriefCase ICH) Sen = 0.936 (0.866-0.976), Spe = 0.923 (0.854-0.966) (1).</p> <p>(BriefCase LVO) Sen = 0.888 (0.819-0.938), Spe = 0.872 (0.825-0.911) (2).</p> <p>(BriefCase BA) Sen = 0.885 (0.804-0.941), Spe = 0.895 (0.84-0.937) (3).</p>	<p>(BriefCase ICH) In 59 TP cases the mean time- to-notification (4.46 min) was 68.11 min faster than mean time-to-exam-open by radiologist (1).</p> <p>(BriefCase LVO) In 111 cases the mean time-to- notification was 3.8 min (2).</p> <p>(BriefCase BA) In 65 TP cases in 2 sites in USA the mean time-to-noti- fication (4.2 min) was 85.2 min faster than mean time-to- exam-open by radiologist (3).</p>	<p>(aidoc) (5) (icobrain-cva) (6, 7)</p>

Table A.6 continued from previous page

Enterprise CTB	<p>Training: 200,000 cases from range of scanners (≥ 5) (8).</p> <p>Validation: 3363 cases (2260 with ICH), $\sim 50\%$ M, mean age ~ 67 [22, >99], Hispanic 5.9-11.3%, Caucasian 76.6-82.1%, other 13.6-19.3%, unknown 2.7-6.9%, 4 different scanners (8).</p>	<p>Training: Image-level labels for ICH subtypes from trained radiologists (8).</p> <p>Validation: Image-level labels for ICH subtypes from 2 ABR-certified and trained neuroradiologists, with a third in case of disagreements (8).</p>	<p>Ensemble of 5 CNNs trained with 5-fold cross validation. 3 heads: classification, left/right localisation, and segmentation. Architectures based on ResNet, Y-Net, and ViT. Single multi-class model with loss function weight for class imbalance, and super-sampling of images with segmentation labels (66).</p>	<p>Results at different binarisation thresholds reported. Second one reported in this table when there are 2 or 3. Thin slice is ≤ 1.5mm and thick slice is > 1.5mm and ≤ 5mm.</p> <p>SDH/EDH: Thin slice: Sen = 0.891 (0.855-0.924), Spe = 0.949 (0.898-0.990). Thick slice: Sen = 0.824 (0.786-0.861), Spe = 0.896 (0.837-0.948) (8).</p> <p>SAH: Thin slice: Sen = 0.939 (0.898-0.973), Spe = 0.965 (0.918-1.00), Thick slice: Sen = 0.874 (0.824-0.918), Spe = 0.962 (0.924-0.990) (8).</p> <p>IAH: Thin slice: Sen = 0.931 (0.908-0.952), Spe = 0.856 (0.811-0.89.6), Thick slice: Sen = 0.903 (0.879-0.925), Spe = 0.903 (0.868-0.938) (8).</p> <p>IVH: Thin slice: Sen = 0.904 (0.836-0.973), Spe = 0.974 (0.935-1.00). Thick slice: Sen = 0.923 (0.868-0.967), Spe = 0.892 (0.828-0.946) (8).</p>	<p>In 277 TP cases across various demographics and locations results showed a triage turnaround time of 81.6 seconds which is similar to the predicate device upon which the FDA approval is based (8).</p>	(9)
-------------------	---	---	--	---	---	-----

Table A.6 continued from previous page

Cina	<p>(CINA-ICH) Training: 8994 ICH cases from multiple hospitals and scanners in the USA (10). Validation: 814 cases (255 with ICH) from multiple hospitals and scanners in the USA, 168 cases age between 18 and 40, 316 between 40 and 70, 249 over 70, and 81 unknown, 206 male, 188 female, 421 unknown (10).</p> <p>(CINA-LVO) Training: 556 LVO cases from multiple hospitals and scanners in USA (10). Validation: 378 cases (156 with LVO) from multiple hospitals and scanners in the USA, 26 cases age between 18 and 40, 176 between 40 and 70, 176 over 70, 185 male, 186 female, 7 unknown (10).</p> <p>(CINA-ASPECTS) Validation: 139 cases (all with acute MCA/ICA occlusion) (11).</p>	<p>(CINA-ICH) Validation: Ground truth from 2 board-certified neuroradiologists with consensus from a third (10).</p> <p>(CINA-LVO) Validation: Ground truth from 2 board-certified neuroradiologists with consensus from a third (10).</p> <p>(CINA-ASPECTS) Validation: Ground truth from 2 board-certified neuroradiologists with consensus from a third (11).</p>	Info not found.	<p>(CINA-ICH) Sen = 0.914, Spe = 0.975, Acc = 0.956 (12).</p> <p>(CINA-LVO) Sen = 0.979, Spe = 0.976, Acc = 0.977 (12).</p> <p>(CINA-ASPECTS) Sen = 0.766, Spe = 0.887, Acc = 0.870 (12).</p>	<p>(CINA-ICH) Time for triage = 22 min (12).</p> <p>(CINA-LVO) Time for triage = 35 min (12).</p>	<p>(CINA-ICH) (CINA-LVO) (10)</p> <p>(CINA-ASPECTS) (11)</p>
e-Stroke	<p>(e-CTA) Training: Over 500 cases (55% with LVO) (67). Validation: 98 consecutive cases (all with acute ischaemic stroke) (13).</p> <p>(e-ASPECTS) Validation: 256 cases (all with acute ischaemic stroke), 8 different USA institutions, median age 71, 45% female (14).</p>	<p>(e-CTA) Validation: Collateral blood flow status scored by 3 neuroradiologists and consensus used as ground truth (13).</p>	(e-CTA) 3D CNN (67).	<p>(e-CTA) 90% agreement with ground truth and ICC of 0.93 (0.90-0.95) (13).</p> <p>(e-ASPECTS) Sen = 0.68 (0.57-0.72), Spe = 0.97 (0.86-0.98), AUC = 0.83 (0.81-0.85) (14).</p>	<p>(e-Stroke) 61 minutes saved for door-in-door-out time (15).</p>	(e-CTA) (13)
BrainScan CT	Training: ~12.5M scans (16).	Info not found.	Info not found.	Info not found.	Info not found.	Info not found.

Table A.6 continued from previous page

Cercare Stroke	Info not found.	Info not found.	CNN used to predict stroke tissue outcome with TRACE DWI, ADC and FLAIR as input channels (17).	Info not found.	Info not found.	(17)
APOLLO BRAIN	Training: 1681 cases (68).	Info not found.	Info not found.	Info not found.	Info not found.	Info not found.
cMRI	Validation: 1399 cases with healthy and diseased brains (91).	Manual segmentation by an expert (91).	ATLAS-based brain region segmentation and rules and intensity based WMH segmentation (91).	(Anatomical region segmentation): DSC (Hippocampus) = 0.88, DSC (Thalamus) = 0.91, DSC (Cortex) = 0.88 (91). (WMH): ICC = 0.97 (91).	Info not found.	(92)
Neuro-Quant	Info not found.	Info not found.	ATLAS-based brain region segmentation (69) and rules and intensity based WMH segmentation (70).	DSC = 0.80-0.90 for major subcortical regions, DSC = 0.75-0.85 for major cortical regions, DSC >0.80 for brain lesions with mean percentage lesion absolute volume difference <2.5% (18).	Info not found.	(19)
DeepCT	Development: 21,603 cases from 3 institutions. Validation: 260 cases (~50% with ICH) from 5 sites (20).	Info not found.	34 layer ResNet, cross-entropy loss, Adam optimiser, rotation and translation data augmentation. Pytorch used (20).	Sen = 0.938 (0.883-0.968), Spe = 0.923 (0.864-0.957) (20).	Processing time = 30.6 (25.8-35.4) seconds from browsing DICOM files to notification (20).	(21)
icobrain	(icobrain-dm/ms) Validation: 1081 (463 MRI, 618 CT) cases including healthy, Alzheimer's, MS, TBI and depression (22). (icobrain-cva) Validation: A clinical dataset and digital phantom (4).	(icobrain-dm/ms) Validation: Ground truth manually labelled or simulated (presumed for longitudinal change) (22).	(icobrain-dm/ms) Unsupervised tissue and lesion segmentation method (71). (icobrain-cva) CNN trained to predict AIF by optimising lesion segmentation objective (7).	(icobrain-dm/ms) MRI: r = 0.91, ICC = 0.90. CT: r = 0.94, ICC = 0.93 (22).	Speed up radiology reading by 40% and improve detection and intra- and inter-rater variability (23).	(23)

Table A.6 continued from previous page

<p>Neuro-Shield</p>	<p>(Volumetry) Training: 186 cases from multiple sites across India with varying magnetic field strength, slice thickness, and scanner manufacturer (84). Validation: 280 cases from the publicly available ADNI dataset (84).</p>	<p>(Volumetry) Training: Ground truth manually labelled in the Hippocampus by experts (84). Validation: Ground truth from public ADNI dataset generated by 3 US board-certified radiologists (84).</p>	<p>(Volumetry) U-Net (84).</p>	<p>(Volumetry) DSC = 0.91 (0.90-0.92), HD = 3.8 (3.57-4.06) (84).</p>	<p>(Volumetry) Saves 80% of radiologists time (85).</p>	<p>(86)</p>
---------------------	--	--	---	---	--	-------------

Table A.6 continued from previous page

<p>MEDIHUB STROKE</p>	<p>(JBS-01K) Validation: Multi-centre (24).</p> <p>(JBS-02K) Training: 50,000 MRI slices. Validation: Single-centre (25).</p> <p>(JBS-03K) Training: 50,000 MRI slices. Validation: Multi-centre (26).</p> <p>(JBS-04K) Validation: Single-centre (27).</p> <p>(JBS-05K) Validation: Single-centre (28).</p> <p>(JBS-11K) Validation: Single-centre (34).</p>	<p>Info not found.</p>	<p>(JBS-01K) 3D CNN for segmentation followed by subtype classification model (24).</p> <p>(JBS-02K) 3D CNN for segmentation followed by severity prediction model (25).</p> <p>(JBS-03K) 3D CNN for segmentation followed by prognosis prediction model (26).</p> <p>(JBS-05K) Ensemble of U-Net and patch U-Net (28).</p>	<p>(JBS-01K) DSC = 0.8356, F1 = 0.8062 (24).</p> <p>(JBS-02K) DSC = 0.8356 (25).</p> <p>(JBS-03K) DSC = 0.8356, AUC = 0.8018 (26).</p> <p>(JBS-04K) AUC = 0.9835 (27).</p> <p>(JBS-05K) AUC = 0.92 (28).</p> <p>(JBS-11K) AUC = 0.9835 (34).</p>	<p>(JBS-01K) Time <40 seconds (24).</p> <p>(JBS-02K) Time <40 seconds (25).</p> <p>(JBS-02K) Time <40 seconds (26).</p> <p>(JBS-04K) Time <10 seconds (27).</p> <p>(JBS-05K) Time <15 seconds (28).</p> <p>(JBS-06K) Time <300 seconds (29).</p> <p>(JBS-07K) Time <300 seconds (30).</p> <p>(JBS-08K) Time <300 seconds (31).</p> <p>(JBS-09K) Time <300 seconds (32).</p> <p>(JBS-10K) Time <300 seconds (33).</p> <p>(JBS-11K) Time <10 seconds (34).</p>	<p>(35)</p>
---------------------------	---	------------------------	---	--	---	-------------

Table A.6 continued from previous page

mdbrain	<p>(Aneurysm detection) Training: Over 100 cases (BA and healthy), multiple Philips scanners (1T, 1.5T and 3T). Validation: 191 cases (54 with aneurysms) from 2 scanners (36).</p> <p>(Volumetry) Training: 2869 cases with equal male/female split (72).</p> <p>(new WMH) Training: 280 cases (73).</p>	<p>(Aneurysm detection) Validation: Ground truth from experienced radiologist (36).</p>	<p>(Aneurysm detection) 3D U-Net (36).</p> <p>(Volumetry) U-Net trained with contrast, resolution, rotation and elastic deformation augmentation (72).</p> <p>(new WMH) 2D U-Net (73).</p>	<p>(Aneurysm detection) Sen = 0.726, Spe = 0.872, Acc = 0.826, PPV = 0.679, NPV = 0.885 (36).</p>	<p>(Brain volumetry) (Lesion characterisation) Median assessment time reduced by 25% (p<0.001) (35).</p>	(37)
Stroke Suite	<p>Training: 24214 cases (38).</p>	Info not found.	Densenet161 (38).	Info not found.	Info not found.	(38)
AQUA	<p>Training: Over 10,000 cases (39) including 300 from 10 scanners (from datasets: ADNI, IXI, PPMI, HCP) for training the anatomical segmentation model (40). Validation: 64 cases including normal and Alzheimer's, 56% USA, 62.5% female, ages 10-90 (40).</p>	<p>Training: Ground truth anatomical labels generated with FreeSurfer and corrected by 4 radiologists (40). Validation: Expert manual segmentation of anatomical regions (40).</p>	<p>(Volumetry) U-Net (74).</p> <p>(WMH) 2D U-Net with bottleneck attention with gaussian noise, affine, elastic and bias field data augmentation, AdamW, learning rate 1e-5 with scheduler, cross-entropy + Dice loss, batch size 64 (75).</p>	<p>DSC = 0.80-0.90 for major sub-cortical regions, DSC = 0.75-0.85 for major cortical regions (40).</p>	Info not found.	(41)
Stroke-Viewer	<p>(LVO) Training: Over 1000 cases from multiple scanners (76).</p>	Info not found.	<p>(LVO) CNN (77).</p>	<p>(ICH) Sen = 0.97, Spe = 0.96 (42).</p> <p>(LVO) Sen = 0.99 (42).</p>	<p>(Stroke-Viewer) 17% reduction in door-to-groin puncture time (42).</p>	Info not found.
Pixyl.Neuro	<p>Validation: 238 cases with healthy, MS, Alzheimer's, micro-angiography and WMH (presumed vascular origin) (82).</p>	Info not found.	Info not found.	<p>(Anatomical region segmentation) DSC = 0.835 ± 0.02 (82).</p> <p>(WMH) DSC = 0.765 ± 0.08 (82).</p>	Info not found.	(83)

Table A.6 continued from previous page

Quantib ND	(Anatomical region segmentation) Validation: 31 cases from multiple scanners (43). (WMH segmentation) Validation: 45 cases with T1(7 with contrast) and FLAIR with various scanner settings (43).	(Anatomical region segmentation) Validation: Manual segmentations (43). (WMH segmentation) Validation: Manual segmentations (43).	Info not found.	(Anatomical region segmentation) DSC = 0.96 ± 0.01 for Brain, DSC = 0.78 ± 0.05 for CSF, DSC = 0.98 ± 0.00 for ICV (43). (WMH segmentation) DSC = 0.61 ± 0.13 (43).	Info not found.	(44)
NEURO- CLOUD VOL	(Anatomical region segmentation) Validation: 135 cases from ADNI (45). (WMH segmentation) Validation: Over 300 cases with 1.5T and 3T scanners, aged 19-65, most with MS (45).	(Anatomical region segmentation) Validation: Manual segmentations from experienced radiologists (45). (WMH segmentation) Manual segmentation from one or more radiology specialists (45).	Multi-stage process involving rule-based and machine learning (45).	(Anatomical region segmentation) Only hippocampus provided. Left: $r = 0.90$ (0.87-0.93), ICC = 0.81 (0.74-0.86). Right: $r = 0.89$ (0.84-0.92), ICC = 0.82 (0.75-0.87) (45). (WMH segmentation) $r = 0.91$, ICC = 0.87 (45).	Info not found.	(46)
qER	Validation: 183 cases with intracranial hyperdensity, 188 cases with midline shift, 210 cases with left lateral ventricle, 210 cases with right lateral ventricle (47).	Validation: Manual segmentation from experts (47).	CNNs (47).	Intracranial hyperdensity: DSC = 0.75 (0.72-0.78), Midline shift: Error = 1.37 ± 1.23 mm. Left lateral ventricle: DSC = 0.79 (0.78-0.81). Right lateral ventricle: DSC = 0.75 (0.73-0.77) (47). Haemorrhage classification: AUC >0.95, ICC = 0.96 (48).	96% reduction in door-to-reporting time (48).	(49)

Table A.6 continued from previous page

Rapid Stroke	<p>(Rapid ICH/Hyperdensity) Training: Large heterogeneous dataset (>1000 cases). Validation: Cases with all types of ICH (excluding haemorrhagic transformations), volume ranging from 0.4-100 ml (50).</p> <p>(Rapid LVO) Validation: 216 cases (107 with LVO), centres in and outside the USA, multiple scanners (53).</p>	<p>(Rapid ICH/Hyperdensity) Training: Ground truth from expert neuroradiologists with > 10y experience. Validation: Ground truth from 3 expert readers (50).</p> <p>(Rapid LVO) Validation: Ground truth from 2 experienced neuroradiologists with review from a 3rd (53).</p>	<p>(Rapid ICH/Hyperdensity) U-Net (50).</p> <p>(Rapid LVO) Traditional machine learning model relying on vessel template and thresholds (81).</p>	<p>(Rapid ICH/Hyperdensity) Sen = 0.981, Spe = 0.997 (50).</p> <p>(Rapid SDH) Sen= 0.924, Spe = 0.987 (52).</p> <p>(Rapid LVO) Sen = 0.97, Spe = 0.96 (53).</p>	<p>(Rapid Stroke) 69% reduction in door-to-CT time, 63% reduction in door-to-CTA time, 52 minute reduction in door-to-decision time, 60% reduction in door-to-out time, 92% reduction in unnecessary transfers, 75% reduction in door-to-groin time, 49% reduction in door-to-needle time (51).</p>	(54, 55)
Digital Brain	Info not found.	Info not found.	Info not found.	Info not found.	Info not found.	(56)

Table A.6 continued from previous page

Viz Radiology Suite	<p>(ICH) Validation: 387 cases (50.6% with ICH), 2 sites in the USA (57).</p> <p>(Aneurysm) Training: 4351 cases (1796 with BA) (78). Validation: 315 cases (21.3% with aneurysm) (58).</p> <p>(Subdural) Training: 1429 cases (251 with SDH) (80), age 62 ± 16, 44% female, 40 scanner types (80). Validation: 542 cases (33.9% with subdural) from 3 sites in the USA (59).</p>	<p>(ICH) Validation: Ground truth from neuro-radiologists (57).</p> <p>(Aneurysm) Ground truth from neuro-radiologists (58).</p> <p>(Subdural) Ground truth from neuro-radiologists (59).</p>	<p>(Aneurysm) Two 3D CNNs. First detects regions of interest and second segments (78).</p> <p>(LVO) 3D CNN followed by random forest (79).</p> <p>(Subdural) 3D CNN (80).</p>	<p>(ICH) Sen = 0.95 (0.91-0.98), Spe = 0.96 (0.92-0.98), AUC = 0.97 (57).</p> <p>(Aneurysm) Sen = 0.93 (0.83-0.98), Spe = 0.89 (0.85-0.93), AUC = 0.967 (0.936-0.997) (58).</p> <p>(Subdural) Sen = 0.94 (0.90-0.97), Spe = 0.92 (0.89-0.95), AUC = 0.96 (59).</p> <p>Reported on website (presumed threshold adjustments):</p> <p>(LVO) Sen = 0.96, Spe = 0.94 (60).</p> <p>(ICH) Sen = 0.85, Spe = 0.99 (60).</p> <p>(Aneurysm) Sen = 0.94, Spe = 0.94 (60).</p> <p>(Subdural) Sen = 0.91, Spe = 0.96 (60).</p>	<p>(LVO) 2.5 day reduction in hospital stay, 73% faster time-to-treatment, 52 mins faster than standard case (61).</p> <p>(ICH) Time to alert specialist = 0.49 ± 0.08 mins down from 18.3 ± 14.2 mins (57).</p> <p>(Aneurysm) Average time to notification = 3.67 mins down from 43.6 mins (58).</p> <p>(Subdural) Time to alert specialist = 1.15 ± 0.57 mins (59).</p>	(62)
VUNO	Info not found.	Manual segmentation by an expert (87).	<p>(Anatomical region segmentation): 2D CNN (88)</p> <p>(WMH): 3D U-Net for brain extraction followed by 2D U-Net, Adam optimiser, learning rate 0.0001, batch size 100, batch normalisation, generalised Dice loss, elastic deformation and mirroring for augmentation (89).</p>	<p>(Anatomical region segmentation): DSC >0.8, ICC >0.965, RVE (Hippocampus) = 0.03 mm^3, RVE (Thalamus) = 0.01 mm^3, RVE (Lateral Ventricle) = 0.01 mm^3 (87).</p> <p>(WMH): DSC >0.8, ICC >0.988 (87).</p>	Info not found.	(90)

Table A.6 continued from previous page

StroCare Suite, AgingCare Suite	(ASPECTS) Training: 557 ischaemic stroke patients from a single institution (95). Validation: 87, 56, and 183 subjects with acute ischaemic stroke, other brain disease, or no disease respectively. Mean ages 67 ± 11 , 66 ± 16 , and 57 ± 14 . 58.6%, 53.6%, and 51.4% male (95).	(ASPECTS) Training: Ground truth manually identified (95). Validation: Consensus between two experts with 10y experience (95).	(ASPECTS) 2D CNN with RNN layers, 5-fold cross validation. (95)	(ICH) Sen = 0.96, Spe = 0.95 (93) (LVO) Sen = 0.92, Spe = 0.93 (93) (ASPECTS) Mean diff = 0.03, Sen = 0.628 (0.585-0.671), Spe = 0.966 (0.962-0.971) (95).	(StroCare Suite) CT to stroke team time reduces from 34 to 19 mins and CT to mechanical thrombectomy time reduced from 154 to 128 minutes (93).	(94)
QP-Brain	Info not found.	Validation: Manual segmentation from and expert (96).	(Anatomical region segmentation) ATLAS based (96).	(Anatomical region segmentation) DSC = 0.983 (0.981-0.986) for gray matter, DSC = 0.990 (0.988-0.992) for white matter, DSC = 0.955 (0.944-0.965) for CSF, DSC = 0.994 (0.994-0.995) for ICV (96). (WMH) DSC = 0.506 (low), DSC = 0.636 (medium), DSC = 0.774 (high), DSC = 0.885 (very high), DSC = 0.692 (average) (96).	(Quibim platforms) 125+ sites working with Quibim. 6/10 top Pharma companies working Quibim. 50+ active clinical studies (97)	(98)
QyScore	(WMH) Validation: WMH lesions loads ranging from 0.09-87.65 ml (99).	Validation: Manual segmentation from and expert (99).	(Anatomical region segmentation) ATLAS based (99).	(Anatomical region segmentation) DSC >0.85 for whole brain regions, DSC 0.75-0.85 for sub-cortical brain regions (99). (WMH) Mean AVD = 3.34 ml (99).	Decreases image reading variability and segmentation errors by 89% (100).	(101)
uAI Discover	Info not found.	Info not found.	Info not found.	Info not found.	Info not found.	(102)

Table A.6 continued from previous page

Pathologies and anatomy:

ICH: intracerebral haemorrhage, (L)VO: (large) vessel occlusion, BA: brain aneurysm, ISL: ischaemic stroke lesion, PVS: enlarged perivascular spaces, SVD: small vessel disease, WMH: white matter hyperintensities, EDH: epidural hematoma, SDH: subdural haemorrhage, SAH: subarachnoid haemorrhage, IVH: intraventricular haemorrhage, IPH: intraparenchymal haemorrhage, ICA: internal carotid artery, MCA: middle cerebral artery.

Modalities:

NCCT: non-contrast computed tomography, CTA: computed tomography angiography, CTP: computed tomography perfusion, MRI: magnetic resonance imaging, T1: T1-weighted MRI, T2: T2-weighted MRI, T2*: T2*-weighted MRI, FLAIR: fluid-attenuated inversion recovery MRI, SWI: susceptibility-weighted imaging MRI, DWI: diffusion-weighted imaging MRI, GRE: gradient echo MRI, TOF: time-of-flight MRI angiography.

Metrics:

AUC: area under the receiver operating characteristic curve, Sen: sensitivity, Spe specificity, Pre precision, DSC: Dice similarity coefficient, r: Pearson's correlation coefficient, TP: true positive, TPR: true positive rate, TNR: true negative rate, R²: coefficient of determination, ICC: intraclass correlation coefficient, Acc: accuracy, Rec: recall, RMSE: root mean square error, HD: Hausdorff distance, RVE: relative volume error, AVD: absolute volume difference.

Other abbreviations:

CNN: convolutional neural network, VIT: vision transformer, AIF: arterial input function

Sources:

- (1) FDA premarket notification: accessdata.fda.gov/cdrh_docs/pdf18/K180647.pdf
- (2) FDA premarket notification: accessdata.fda.gov/cdrh_docs/pdf19/K192383.pdf
- (3) FDA premarket notification: accessdata.fda.gov/cdrh_docs/pdf21/K213721.pdf
- (4) FDA premarket notification: accessdata.fda.gov/cdrh_docs/pdf19/K192962.pdf
- (5) Several clinical studies linked via website: aidoc.com/learn/clinical-studies/
- (6) [de la Rosa et al. \(2020\)](#)
- (7) [de la Rosa et al. \(2021\)](#)
- (8) FDA premarket notification: accessdata.fda.gov/cdrh_docs/pdf22/K223240.pdf
- (9) Several clinical studies linked via website: annalise.ai/clinical-evidence/ and annalise.ai/case-studies/
- (10) [McLouth et al. \(2021\)](#)
- (11) [Ayobi et al. \(2023\)](#)
- (12) Avicenna.ai website: avicenna.ai/solutions/ai-tools-for-neuro/
- (13) [Grunwald et al. \(2019\)](#)
- (14) FDA premarket notification: accessdata.fda.gov/cdrh_docs/pdf22/K221564.pdf
- (15) BRAINOMIX 360 brochure: brainomix.com/media/ozbfjclx/11-x-17-bi-fold-combined.pdf
- (16) BRAINSCAN.AI website: brainscan.ai/company.html
- (17) Publication linked on website under stroke filter: cercare-medical.com/resources?tag=stroke#publications-list
- (18) FDA premarket notification: accessdata.fda.gov/cdrh_docs/pdf17/K170981.pdf
- (19) Publication linked on website: cortechs.ai/insight/category/published-research/
- (20) FDA premarket notification: accessdata.fda.gov/cdrh_docs/pdf18/K182875.pdf
- (21) Publications linked on website: deep01.com/publications
- (22) FDA premarket notification: accessdata.fda.gov/cdrh_docs/pdf19/K192130.pdf
- (23) icometrix website with several linked publications under each sub-product: icometrix.com/services
- (24) JBS-01K brochure: jlkgroup.com/pdf/en/JBS-01K_eng.pdf
- (25) JBS-02K brochure: jlkgroup.com/pdf/en/JBS-02K_eng.pdf
- (26) JBS-03K brochure: jlkgroup.com/pdf/en/JBS-03K_eng.pdf
- (27) JBS-04K brochure: jlkgroup.com/pdf/en/JBS-04K_eng.pdf
- (28) JBS-05K brochure: jlkgroup.com/pdf/en/JBS-05K_eng.pdf
- (29) JBS-06K brochure: jlkgroup.com/pdf/en/JBS-06K_eng.pdf
- (30) JBS-07K brochure: jlkgroup.com/pdf/en/JBS-07K_eng.pdf
- (31) JBS-08K brochure: jlkgroup.com/pdf/en/JBS-08K_eng.pdf
- (32) JBS-09K brochure: jlkgroup.com/pdf/en/JBS-09K_eng.pdf

Table A.6 continued from previous page

- (33) JBS-10K brochure: jlkgroup.com/pdf/en/JBS-10K_eng.pdf
- (34) JBS-11K brochure: jlkgroup.com/pdf/en/JBS-11K_eng.pdf
- (35) abstract on mediare website: mediaire.ai/en/real-life-evaluation-of-the-ai-based-neuroradiology-suite-mdbrain/
- (36) [Lehnen et al. \(2022\)](#)
- (37) Publications linked on website: mediaire.ai/en/publications/
- (38) [Olive-Gadea et al. \(2020\)](#)
- (39) neurophet website: neurophet.com/Products/AQUA
- (40) FDA premarket notification: accessdata.fda.gov/cdrh_docs/pdf22/K220437.pdf
- (41) Publication linked on website: neurophet.com/Tech/Publications
- (42) NICOLAB website: nicolab.com/strokeviewer/ai-portfolio/
- (43) FDA premarket notification: accessdata.fda.gov/cdrh_docs/pdf21/K213737.pdf
- (44) Publications linked on website: quantib.com/resources/publications
- (45) Whitepaper available at: qubiotech.com/en/resources/#whitepapers
- (46) Publications linked on website: qubiotech.com/en/resources/#publications
- (47) FDA premarket notification: accessdata.fda.gov/cdrh_docs/pdf21/K211222.pdf
- (48) qure.ai website: qure.ai/product/qer
- (49) Publications linked on website: qure.ai/evidences
- (50) Rapid ICH/Hyperdensity whitepaper available at: rapidai.com/rapid-ich-hyperdensity
- (51) RapidAI website: rapidai.com/stroke
- (52) RapidAI website: rapidai.com/rapid-sdh
- (53) RapidAI website: rapidai.com/rapid-lvo
- (54) Publications linked on website: rapidai.com/publications
- (55) Clinical trials linked on website: rapidai.com/trials
- (56) Publications linked on website: en.shukun.net/scientific.html
- (57) FDA premarket notification: accessdata.fda.gov/cdrh_docs/pdf21/K210209.pdf
- (58) FDA premarket notification: accessdata.fda.gov/cdrh_docs/pdf21/K213319.pdf
- (59) FDA premarket notification: accessdata.fda.gov/cdrh_docs/pdf22/K220439.pdf
- (60) Viz AI website: viz.ai/neuro
- (61) Viz AI website: viz.ai/large-vessel-occlusion
- (62) Publication linked on website: viz.ai/publications
- (63) [Ojeda et al. \(2019\)](#)
- (64) [Kundisch et al. \(2021\)](#)
- (65) [Soun et al. \(2021\)](#)
- (66) [Buchlak et al. \(2023\)](#)
- (67) [Weyland et al. \(2022\)](#)
- (68) [Krag et al. \(2023\)](#)
- (69) Whitepaper downloaded from: cortechs.ai/insight/whitepaper-dynamic-atlas/
- (70) Whitepaper downloaded from: cortechs.ai/insight/whitepaper-lesionquant-performance-evaluation-accuracy-and-reproducibility-2/
- (71) [Beadnall et al. \(2019\)](#)
- (72) [Purrer et al. \(2023\)](#)
- (73) [Dalbis et al. \(2022\)](#)
- (74) [Kim et al. \(2023b\)](#)

Table A.6 continued from previous page

- (75) [Lee et al. \(2023\)](#)
- (76) [Bruggeman et al. \(2022\)](#)
- (77) [Yang et al. \(2023\)](#)
- (78) [Kim et al. \(2023a\)](#)
- (79) [Delora et al. \(2023\)](#)
- (80) [Colasurdo et al. \(2022\)](#)
- (81) [Schlossman et al. \(2022\)](#)
- (82) FDA premarket notification: accessdata.fda.gov/cdrh_docs/pdf21/K213253.pdf
- (83) Publications linked on website: pixyl.ai/publications/
- (84) FDA premarket notification: accessdata.fda.gov/cdrh_docs/pdf22/K220034.pdf
- (85) INMED AI website: inmed.ai/neuroshieldmr/
- (86) Publications linked on website: inmed.ai/research/
- (87) FDA premarket notification: accessdata.fda.gov/cdrh_docs/pdf23/K231398.pdf
- (88) [Kim et al. \(2022\)](#)
- (89) [Joo et al. \(2022\)](#)
- (90) Publications linked on website: vuno.co/en/publication
- (91) FDA premarket notification: accessdata.fda.gov/cdrh_docs/pdf17/K171328.pdf
- (92) Publications linked on website: combinostics.com/publications/
- (95) [Lee et al. \(2024\)](#)
- (96) FDA premarket notification: accessdata.fda.gov/cdrh_docs/pdf23/K232231.pdf
- (97) Quibim website: quibim.com/platform/
- (98) Publications linked on website: quibim.com/info-hub/
- (99) FDA premarket notification: accessdata.fda.gov/cdrh_docs/pdf19/K192531.pdf
- (100) QYNAPSE website: qynapse.com/qyscore/
- (101) Publications linked on website: qynapse.com/publications/
- (102) Publication linked on website: uii-ai.com/achievements.html#t

References

- Abbasi, H., Orouskhani, M., Asgari, S., Zadeh, S.S., 2023. Automatic brain ischemic stroke segmentation with deep learning: A review. *Neurosci. Inform.* , 100145.
- Arboix, A., 2015. Cardiovascular risk factors for acute stroke: Risk profiles in the different subtypes of ischemic stroke. *World J. Clin. Cases* 3, 418.
- Ayobi, A., Chang, P., Chow, D., Filippi, C., Quenet, S., Tassy, M., Chaibi, Y., 2023. Validation of a deep learning AI-based software for automated ASPECTS assessment. *European Congress of Radiology (ECR)*. doi:[10.26044/ecr2023/C-19206](https://doi.org/10.26044/ecr2023/C-19206). scientific Exhibit, poster C-19206.
- Balakrishnan, R., Hernández, M.d.C.V., Farrall, A.J., 2021. Automatic segmentation of white matter hyperintensities from brain magnetic resonance images in the era of deep learning and big data—a systematic review. *Comp. Med. Imaging Graphics* 88, 101867.
- Barber, P.A., Demchuk, A.M., Zhang, J., Buchan, A.M., 2000. Validity and reliability of a quantitative computed tomography score in predicting outcome of hyperacute stroke before thrombolytic therapy. *The Lancet* 355, 1670–1674.
- Barisano, G., Lynch, K.M., Sibia, F., Lan, H., Shih, N.C., Sepehrband, F., Choupan, J., 2022. Imaging perivascular space structure and function using brain mri. *Neuroimage* 257, 119329.
- Beadnall, H., Wang, C., Van Hecke, W., Ribbens, A., Billiet, T., Barnett, M., 2019. Comparing longitudinal brain atrophy measurement techniques in a real-world multiple sclerosis clinical practice cohort: towards clinical integration? *Therapeutic advances in neurological disorders* 12, 1756286418823462.
- Billot, B., Greve, D.N., Puonti, O., Thielscher, A., Van Leemput, K., Fischl, B., Dalca, A.V., Iglesias, J.E., et al., 2023. Synthseg: Segmentation of brain mri scans of any contrast and resolution without retraining. *Medical image analysis* 86, 102789.
- Bivard, A., Churilov, L., Parsons, M., 2020. Artificial intelligence for decision support in acute stroke—current roles and potential. *Nat. Rev. Neurol.* 16, 575–585.

- Bruggeman, A.A., Koopman, M.S., Soomro, J., Small, J.E., Yoo, A.J., Marquering, H.A., Emmer, B.J., 2022. Automated detection and location specification of large vessel occlusion on computed tomography angiography in acute ischemic stroke. *Stroke: Vascular and Interventional Neurology* 2, e000158.
- Buchlak, Q.D., Tang, C.H., Seah, J.C., Johnson, A., Holt, X., Bottrell, G.M., Wardman, J.B., Samarasinghe, G., Dos Santos Pinheiro, L., Xia, H., et al., 2023. Effects of a comprehensive brain computed tomography deep learning model on radiologist detection accuracy. *European Radiology* , 1–13.
- Colasurdo, M., Leibushor, N., Robledo, A., Vasandani, V., Luna, Z.A., Rao, A.S., Garcia, R., Srinivasan, V.M., Sheth, S.A., Avni, N., et al., 2022. Automated detection and analysis of subdural hematomas using a machine learning algorithm. *J. Neurosurg.* 1, 1–8.
- Commowick, O., Kain, M., Casey, R., Ameli, R., Ferré, J.C., Kerbrat, A., Tourdias, T., Cervenansky, F., Camarasu-Pop, S., Glatard, T., et al., 2021. Multiple sclerosis lesions segmentation from multiple experts: The miccai 2016 challenge dataset. *Neuroimage* 244, 118589.
- Cox, R.W., 1996. Afni: software for analysis and visualization of functional magnetic resonance neuroimages. *Computers and Biomedical research* 29, 162–173.
- Dalbis, T., Grilo, J., Hitziger, S., Ling, W.X., Opalka, J.R., Lemke, A., 2022. Deep learning-based detection and segmentation of new MS lesions using optimized merging of orientations. *European Congress of Radiology (ECR)*. URL: <https://epos.myesr.org/poster/esr/ecr2022/C-22102>, doi:10.26044/ecr2022/C-22102. publisher: European Congress of Radiology - ECR 2022.
- Debette, S., Markus, H., 2010. The clinical importance of white matter hyperintensities on brain magnetic resonance imaging: systematic review and meta-analysis. *Br. Med. J.* 341.
- Delora, A., Hadjialiakbari, C., Percenti, E., Torres, J., Alderazi, Y.J., Ezzeldin, R., Hassan, A.E., Ezzeldin, M., 2023. Viz lvo versus rapid lvo in detection of large vessel occlusion on ct angiography for acute stroke. *J. Neurointerventional Surg.* .

- Donkor, E.S., et al., 2018. Stroke in the century: a snapshot of the burden, epidemiology, and quality of life. *Stroke Res. Treat.* 2018.
- Dosovitskiy, A., Beyer, L., Kolesnikov, A., Weissenborn, D., Zhai, X., Unterthiner, T., Dehghani, M., Minderer, M., Heigold, G., Gelly, S., et al., 2020. An image is worth 16x16 words: Transformers for image recognition at scale. *arXiv preprint arXiv:2010.11929* .
- Duan, Y., Shan, W., Liu, L., Wang, Q., Wu, Z., Liu, P., Ji, J., Liu, Y., He, K., Wang, Y., 2020. Primary categorizing and masking cerebral small vessel disease based on “deep learning system”. *Front. Neuroinformatics* 14, 17.
- Duering, M., Biessels, G.J., Brodtmann, A., Chen, C., Cordonnier, C., de Leeuw, F.E., Debette, S., Frayne, R., Jouvent, E., Rost, N.S., et al., 2023. Neuroimaging standards for research into small vessel disease—advances since 2013. *The Lancet Neurology* 22, 602–618.
- Feigin, V.L., Brainin, M., Norrving, B., Martins, S., Sacco, R.L., Hacke, W., Fisher, M., Pandian, J., Lindsay, P., 2022. World stroke organization (wso): global stroke fact sheet 2022. *Int. J. Stroke* 17, 18–29.
- Feigin, V.L., Stark, B.A., Johnson, C.O., Roth, G.A., Bisignano, C., Abady, G.G., Abbasifard, M., Abbasi-Kangevari, M., Abd-Allah, F., Abedi, V., et al., 2021. Global, regional, and national burden of stroke and its risk factors, 1990–2019: a systematic analysis for the global burden of disease study 2019. *The Lancet Neurology* 20, 795–820.
- Ferlin, M., Klawikowska, Z., Grochowski, M., Grzywińska, M., Szurowska, E., 2023. Exploring the landscape of automatic cerebral microbleed detection: A comprehensive review of algorithms, current trends, and future challenges. *Expert Systems with Applications* 232, 120655.
- Flanders, A.E., Prevedello, L.M., Shih, G., Halabi, S.S., Kalpathy-Cramer, J., Ball, R., Mongan, J.T., Stein, A., Kitamura, F.C., Lungren, M.P., et al., 2020. Construction of a machine learning dataset through collaboration: the rsna 2019 brain ct hemorrhage challenge. *Radiol.: Artif. Intell.* 2, e190211.

- Girshick, R., Donahue, J., Darrell, T., Malik, J., 2014. Rich feature hierarchies for accurate object detection and semantic segmentation, in: Proceedings of the IEEE conference on computer vision and pattern recognition, pp. 580–587.
- Grunwald, I.Q., Kulikovski, J., Reith, W., Gerry, S., Namias, R., Politi, M., Papanagiotou, P., Essig, M., Mathur, S., Joly, O., et al., 2019. Collateral automation for triage in stroke: evaluating automated scoring of collaterals in acute stroke on computed tomography scans. *Cerebrovascular Diseases* 47, 217–222.
- Guerrero, R., Qin, C., Oktay, O., Bowles, C., Chen, L., Joules, R., Wolz, R., Valdés-Hernández, M.d.C., Dickie, D.A., Wardlaw, J., et al., 2018. White matter hyperintensity and stroke lesion segmentation and differentiation using convolutional neural networks. *NeuroImage: Clin.* 17, 918–934.
- He, K., Zhang, X., Ren, S., Sun, J., 2016. Deep residual learning for image recognition, in: Proceedings of the IEEE conference on computer vision and pattern recognition, pp. 770–778.
- Henderson, M., 2022. URL: <https://www.rsna.org/news/2022/may/global-radiologist-shortage>.
- Hernandez Petzsche, M.R., de la Rosa, E., Hanning, U., Wiest, R., Valenzuela, W., Reyes, M., Meyer, M., Liew, S.L., Kofler, F., Ezhov, I., et al., 2022. Isles 2022: A multi-center magnetic resonance imaging stroke lesion segmentation dataset. *Sci. Data* 9, 762.
- Huang, G., Liu, Z., Van Der Maaten, L., Weinberger, K.Q., 2017. Densely connected convolutional networks, in: Proceedings of the IEEE conference on computer vision and pattern recognition, pp. 4700–4708.
- Isensee, F., Jaeger, P.F., Kohl, S.A., Petersen, J., Maier-Hein, K.H., 2021. nnu-net: a self-configuring method for deep learning-based biomedical image segmentation. *Nature methods* 18, 203–211.
- Isensee, F., Schell, M., Pflueger, I., Brugnara, G., Bonekamp, D., Neuberger, U., Wick, A., Schlemmer, H.P., Heiland, S., Wick, W., et al., 2019. Automated brain extraction of multisequence mri using artificial neural networks. *Hum. Brain Mapp.* 40, 4952–4964.

- Jenkinson, M., Bannister, P., Brady, M., Smith, S., 2002. Improved optimization for the robust and accurate linear registration and motion correction of brain images. *Neuroimage* 17, 825–841.
- Jenkinson, M., Smith, S., 2001. A global optimisation method for robust affine registration of brain images. *Med. Image Anal.* 5, 143–156.
- Jiang, J., Wang, D., Song, Y., Sachdev, P.S., Wen, W., 2022. Computer-aided extraction of select mri markers of cerebral small vessel disease: A systematic review. *NeuroImage* , 119528.
- Joo, L., Shim, W.H., Suh, C.H., Lim, S.J., Heo, H., Kim, W.S., Hong, E., Lee, D., Sung, J., Lim, J.S., et al., 2022. Diagnostic performance of deep learning-based automatic white matter hyperintensity segmentation for classification of the fazekas scale and differentiation of subcortical vascular dementia. *Plos one* 17, e0274562.
- Kim, H.W., Ballekere, A., Ali, I., Marioni, S.S., Abdelkhaleq, R., Niktabe, A., Azeem, H., Iyyangar, A., Segev, O., Bibas, O., et al., 2023a. Machine learning-enabled detection of unruptured cerebral aneurysms improves detection rates and clinical care. *Stroke: Vascular and Interventional Neurology* 3, e000938.
- Kim, J., Oh, S.W., Kim, J.Y., Kim, R.E., Kim, D., 2023b. Comparative study of two commercial brain volumetry software: Assessing medial temporal lobe atrophy .
- Kim, J.S., Han, J.W., Bae, J.B., Moon, D.G., Shin, J., Kong, J.E., Lee, H., Yang, H.W., Lim, E., Kim, J.Y., et al., 2022. Deep learning-based diagnosis of alzheimer’s disease using brain magnetic resonance images: an empirical study. *Scientific Reports* 12, 18007.
- Krag, C.H., Müller, F.C., Gandrup, K.L., Raaschou, H., Andersen, M.B., Brejneboel, M.W., Sagar, M.V., Bojsen, J.A., Rasmussen, B.S., Graumann, O., et al., 2023. Diagnostic test accuracy study of a commercially available deep learning algorithm for ischemic lesion detection on brain mris in suspected stroke patients from a non-comprehensive stroke center. *European Journal of Radiology* 168, 111126.
- Kuijff, H.J., Biesbroek, J.M., De Bresser, J., Heinen, R., Andermatt, S., Bento, M., Berseth, M., Belyaev, M., Cardoso, M.J., Casamitjana, A.,

- et al., 2019. Standardized assessment of automatic segmentation of white matter hyperintensities and results of the wmh segmentation challenge. *IEEE Trans. Med. Imaging* 38, 2556–2568.
- Kundisch, A., Hönning, A., Mutze, S., Kreissl, L., Spohn, F., Lemcke, J., Sitz, M., Sparenberg, P., Goelz, L., 2021. Deep learning algorithm in detecting intracranial hemorrhages on emergency computed tomographies. *PLoS One* 16, e0260560.
- Lansberg, M.G., Albers, G.W., Beaulieu, C., Marks, M.P., 2000. Comparison of diffusion-weighted mri and ct in acute stroke. *Neurology* 54, 1557–1561.
- LeCun, Y., Boser, B., Denker, J.S., Henderson, D., Howard, R.E., Hubbard, W., Jackel, L.D., 1989. Backpropagation applied to handwritten zip code recognition. *Neural computation* 1, 541–551.
- Lee, S., Rieu, Z., Kim, R.E., Lee, M., Yen, K., Yong, J., Kim, D., 2023. Automatic segmentation of white matter hyperintensities in t2-flair with aqua: a comparative validation study against conventional methods. *Brain Research Bulletin* , 110825.
- Lee, S.J., Park, G., Kim, D., Jung, S., Song, S., Hong, J.M., Shin, D.H., Lee, J.S., 2024. Clinical evaluation of a deep-learning model for automatic scoring of the alberta stroke program early ct score on non-contrast ct. *Journal of NeuroInterventional Surgery* 16, 61–66.
- Lehnen, N., Haase, R., Schmeel, F., Vatter, H., Dorn, F., Radbruch, A., Paech, D., 2022. Automated detection of cerebral aneurysms on tof-mra using a deep learning approach: An external validation study. *Am. J. Neuroradiol.* 43, 1700–1705.
- Liu, L., Chen, S., Zhu, X., Zhao, X.M., Wu, F.X., Wang, J., 2020a. Deep convolutional neural network for accurate segmentation and quantification of white matter hyperintensities. *Neurocomputing* 384, 231–242.
- Liu, L., Kurgan, L., Wu, F.X., Wang, J., 2020b. Attention convolutional neural network for accurate segmentation and quantification of lesions in ischemic stroke disease. *Med. Image Anal.* 65, 101791.

- Liu, L., Wang, Y., Chang, J., Zhang, P., Liang, G., Zhang, H., 2022. Llrhnet: multiple lesions segmentation using local-long range features. *Frontiers in Neuroinformatics* 16, 859973.
- Liu, Y., Li, X., Li, T., Li, B., Wang, Z., Gan, J., Wei, B., 2021. A deep semantic segmentation correction network for multi-model tiny lesion areas detection. *BMC Medical Informatics and Decision Making* 21, 1–9.
- Llambias, S.N., Nielsen, M., Ghazi, M.M., 2024. Heterogeneous learning for brain lesion segmentation, detection, and classification, in: *Northern Lights Deep Learning Conference 2024*.
- Maes, F., Collignon, A., Vandermeulen, D., Marchal, G., Suetens, P., 1997. Multimodality image registration by maximization of mutual information. *IEEE Trans. Med. Imaging* 16, 187–198.
- Maier-Hein, L., Reinke, A., Godau, P., Tizabi, M.D., Buettner, F., Christodoulou, E., Glocker, B., Isensee, F., Kleesiek, J., Kozubek, M., et al., 2024. Metrics reloaded: recommendations for image analysis validation. *Nat. Methods* , 1–18.
- McLouth, J., Elstrott, S., Chaibi, Y., Quenet, S., Chang, P.D., Chow, D.S., Soun, J.E., 2021. Validation of a deep learning tool in the detection of intracranial hemorrhage and large vessel occlusion. *Front. Neurol.* 12, 656112.
- Mikhail, P., Le, M.G.D., Mair, G., 2020. Computational image analysis of nonenhanced computed tomography for acute ischaemic stroke: a systematic review. *J. Stroke Cerebrovasc. Dis.* 29, 104715.
- MONAI Consortium, M., et al., 2020. Monai: Medical open network for ai. Online at <https://doi.org/10.5281/zenodo.5525502>.
- Murray, N.M., Unberath, M., Hager, G.D., Hui, F.K., 2020. Artificial intelligence to diagnose ischemic stroke and identify large vessel occlusions: a systematic review. *J. Neurointerventional Surg.* 12, 156–164.
- Ojeda, P., Zawaideh, M., Mossa-Basha, M., Haynor, D., 2019. The utility of deep learning: evaluation of a convolutional neural network for detection of intracranial bleeds on non-contrast head computed tomography studies, in: *Medical Imaging 2019: Image Processing*, SPIE. pp. 899–906.

- Olive-Gadea, M., Crespo, C., Granes, C., Hernandez-Perez, M., Perez de la Ossa, N., Laredo, C., Urrea, X., Carlos Soler, J., Soler, A., Puyalto, P., et al., 2020. Deep learning based software to identify large vessel occlusion on noncontrast computed tomography. *Stroke* 51, 3133–3137.
- Olthof, A.W., van Ooijen, P.M., Rezazade Mehrizi, M.H., 2020. Promises of artificial intelligence in neuroradiology: a systematic technographic review. *Neuroradiology* 62, 1265–1278.
- Pham, W., Lynch, M., Spitz, G., O’Brien, T., Vivash, L., Sinclair, B., Law, M., 2022. A critical guide to the automated quantification of perivascular spaces in magnetic resonance imaging. *Front. Neurosci.* 16, 1021311.
- Phitidis, J., O’Neil, A.Q., Wiseman, S., Dickie, D.A., Sakka, E., Kampaite, A., Whiteley, W., Bernabeu, M.O., Alex, B., Wardlaw, J.M., et al., 2023. Segmentation of white matter hyperintensities and ischaemic stroke lesions in structural mri, in: *Annual Conference on Medical Image Understanding and Analysis*, Springer. pp. 3–17.
- Purrer, V., Pohl, E., Lueckel, J.M., Borger, V., Sauer, M., Radbruch, A., Wüllner, U., Schmeel, F.C., 2023. Artificial-intelligence-based mri brain volumetry in patients with essential tremor and tremor-dominant parkinson’s disease. *Brain Communications* 5, fcad271.
- Reinke, A., Tizabi, M.D., Baumgartner, M., Eisenmann, M., Heckmann-Nötzel, D., Kavur, A.E., Rädtsch, T., Sudre, C.H., Acion, L., Antonelli, M., et al., 2024. Understanding metric-related pitfalls in image analysis validation. *Nat. Methods.* , 1–13.
- Ronneberger, O., Fischer, P., Brox, T., 2015. U-net: Convolutional networks for biomedical image segmentation, in: *Medical Image Computing and Computer-Assisted Intervention–MICCAI 2015: 18th International Conference, Munich, Germany, October 5-9, 2015, Proceedings, Part III* 18, Springer. pp. 234–241.
- de la Rosa, E., Robben, D., Sima, D.M., Kirschke, J.S., Menze, B., 2020. Differentiable deconvolution for improved stroke perfusion analysis, in: *Medical Image Computing and Computer Assisted Intervention–MICCAI 2020: 23rd International Conference, Lima, Peru, October 4–8, 2020, Proceedings, Part VII* 23, Springer. pp. 593–602.

- de la Rosa, E., Sima, D.M., Menze, B., Kirschke, J.S., Robben, D., 2021. Aifnet: Automatic vascular function estimation for perfusion analysis using deep learning. *Med. Image Anal.* 74, 102211.
- Schlossman, J., Ro, D., Salehi, S., Chow, D., Yu, W., Chang, P.D., Soun, J.E., 2022. Head-to-head comparison of commercial artificial intelligence solutions for detection of large vessel occlusion at a comprehensive stroke center. *Front. Neurol.* 13, 2315.
- Shi, L., Wang, D., Liu, S., Pu, Y., Wang, Y., Chu, W.C., Ahuja, A.T., Wang, Y., 2013. Automated quantification of white matter lesion in magnetic resonance imaging of patients with acute infarction. *J. Neurosci. Methods* 213, 138–146.
- Shi, Y., Wardlaw, J.M., 2016. Update on cerebral small vessel disease: a dynamic whole-brain disease. *Stroke and Vasc. Neurol.* 1.
- Sled, J.G., Zijdenbos, A.P., Evans, A.C., 1998. A nonparametric method for automatic correction of intensity nonuniformity in mri data. *IEEE Trans. Med. Imaging* 17, 87–97.
- Smith, S.M., 2002. Fast robust automated brain extraction. *Hum. Brain Mapp.* 17, 143–155.
- Soun, J., Chow, D., Nagamine, M., Takhtawala, R., Filippi, C., Yu, W., Chang, P., 2021. Artificial intelligence and acute stroke imaging. *Am. J. Neuroradiol.* 42, 2–11.
- Styner, M., Lee, J., Chin, B., Chin, M., Commowick, O., Tran, H., Markovic-Plese, S., Jewells, V., Warfield, S., 2008. 3d segmentation in the clinic: A grand challenge ii: Ms lesion segmentation. *MIDAS journal* 2008, 1–6.
- Sudre, C.H., Anson, B.G., Ingala, S., Lane, C.D., Jimenez, D., Haider, L., Varsavsky, T., Smith, L., Ourselin, S., Jäger, R.H., et al., 2019. 3d multirater rnn for multimodal multiclass detection and characterisation of extremely small objects, in: *International Conference on Medical Imaging with Deep Learning*, PMLR. pp. 447–456.
- Sudre, C.H., Van Wijnen, K., Dubost, F., Adams, H., Atkinson, D., Barkhof, F., Birhanu, M.A., Bron, E.E., Camarasa, R., Chaturvedi, N., et al., 2023.

- Where is valdo? vascular lesions detection and segmentation challenge at miccai 2021. *Med. Image Anal.* , 103029.
- Tanabe, J., 2011. White matter hyperintensities are associated with an increased risk of stroke, dementia and mortality. *Evidence-based Ment. Health* 14, 1.
- Tsai, J.Z., Peng, S.J., Chen, Y.W., Wang, K.W., Li, C.H., Wang, J.Y., Chen, C.J., Lin, H.J., Smith, E.E., Wu, H.K., et al., 2014. Automated segmentation and quantification of white matter hyperintensities in acute ischemic stroke patients with cerebral infarction. *PloS one* 9, e104011.
- Tustison, N.J., Avants, B.B., Cook, P.A., Zheng, Y., Egan, A., Yushkevich, P.A., Gee, J.C., 2010. N4itk: improved n3 bias correction. *IEEE transactions on medical imaging* 29, 1310–1320.
- Uchiyama, Y., Asano, T., Hara, T., Fujita, H., Hoshi, H., Iwama, T., Kinoshada, Y., 2009. Cad scheme for differential diagnosis of lacunar infarcts and normal virchow-robin spaces on brain mr images, in: *World Congress on Medical Physics and Biomedical Engineering, September 7-12, 2009, Munich, Germany: Vol. 25/5 Information and Communication in Medicine, Telemedicine and e-Health*, Springer. pp. 126–128.
- Uchiyama, Y., Kunieda, T., Asano, T., Kato, H., Hara, T., Kanematsu, M., Iwama, T., Hoshi, H., Kinoshada, Y., Fujita, H., 2008. Computer-aided diagnosis scheme for classification of lacunar infarcts and enlarged virchow-robin spaces in brain mr images, in: *2008 30th Annual International Conference of the IEEE Engineering in Medicine and Biology Society, IEEE*. pp. 3908–3911.
- Vaswani, A., Shazeer, N., Parmar, N., Uszkoreit, J., Jones, L., Gomez, A.N., Kaiser, Ł., Polosukhin, I., 2017. Attention is all you need, in: *Guyon, I., Luxburg, U.V., Bengio, S., Wallach, H., Fergus, R., Vishwanathan, S., Garnett, R. (Eds.), Advances in Neural Information Processing Systems*, Curran Associates, Inc.
- Wang, X., Shen, T., Yang, S., Lan, J., Xu, Y., Wang, M., Zhang, J., Han, X., 2021. A deep learning algorithm for automatic detection and classification of acute intracranial hemorrhages in head ct scans. *Neuroimage: Clin.* 32, 102785.

- Wang, Y., Catindig, J.A., Hilal, S., Soon, H.W., Ting, E., Wong, T.Y., Venkatasubramanian, N., Chen, C., Qiu, A., 2012. Multi-stage segmentation of white matter hyperintensity, cortical and lacunar infarcts. *Neuroimage* 60, 2379–2388.
- Wardlaw, J.M., Mair, G., Von Kummer, R., Williams, M.C., Li, W., Storkey, A.J., Trucco, E., Liebeskind, D.S., Farrall, A., Bath, P.M., et al., 2022. Accuracy of automated computer-aided diagnosis for stroke imaging: a critical evaluation of current evidence. *Stroke* 53, 2393–2403.
- Waymont, J.M., Valdes Hernandez, M.D.C., Bernal, J., Duarte Coello, R., Brown, R., Ballerini, L., Chappell, F.M., Wardlaw, J.M., 2024. A systematic review and meta-analysis of automated methods for quantifying enlarged perivascular spaces in the brain. *medRxiv* , 2024–03.
- Weyland, C.S., Papanagiotou, P., Schmitt, N., Joly, O., Bellot, P., Mokli, Y., Ringleb, P.A., Kastrup, A., Möhlenbruch, M.A., Bendszus, M., et al., 2022. Hyperdense artery sign in patients with acute ischemic stroke—automated detection with artificial intelligence-driven software. *Front. Neurol.* 13, 807145.
- Yang, W., Soomro, J., Jansen, I.G., Venkatesh, A., Yoo, A.J., Lopes, D., Beenen, L.F., Emmer, B.J., Majoie, C.B., Marquering, H.A., 2023. Collateral capacity assessment: Robustness and interobserver agreement of two grading scales and agreement with quantitative scoring. *Clinical neuroradiology* 33, 353–359.
- Yao, A.D., Cheng, D.L., Pan, I., Kitamura, F., 2020. Deep learning in neuroradiology: a systematic review of current algorithms and approaches for the new wave of imaging technology. *Radiol.: Artif. Intell.* 2, e190026.
- Yearley, A.G., Goedmakers, C.M., Panahi, A., Rana, A., Doucette, J., Ranganathan, K., Smith, T.R., 2023. Fda-approved machine learning algorithms in neuroradiology: A systematic review of the current evidence for approval. *Artif. Intell. Med.* , 102607.
- Yeo, M., Tahayori, B., Kok, H.K., Maingard, J., Kutaiba, N., Russell, J., Thijs, V., Jhamb, A., Chandra, R.V., Brooks, M., et al., 2021. Review of deep learning algorithms for the automatic detection of intracranial hemorrhages on computed tomography head imaging. *J. Neurointerventional Surg.* 13, 369–378.